scientific reports

Check for updates

OPEN

Soil nitrous oxide and methane emissions in contrasting land use of the West African Sudanian savanna

Francis E. Oussou[1,2,3]✉, Ralf Kiese[4], Souleymane Sy[3], Jan Bliefernicht[3], Ines Spangenberg[3,4], Samuel Guug[3,5,6], Anja Schäfler-Schmid[4], Rainer Steinbrecher[4], Frank Neidl[4], Michael Ayamba[5], Luitpold Hingerl[3,4], Emmanuel Quansah[6], Alex Frempong[6], Patrick Davies[6], Windmanagda Sawadogo[3,4], Christiana F. Olusegun[7], Ricky. M. Mwanake[4], Nicaise Yalo[2], Yinusa A. Asiwaju-Bello[8], Moussa Boukari[2], Leonard K. Amekudzi[6], Kehinde Ogunjobi[5] & Harald Kunstmann[3,4,9]✉

Changes in land use and land management can have significant effects on the global emissions budget, influencing the climate through biogeochemical processes. However, their impacts on major soil greenhouse gas (GHG) emissions in West Africa remain poorly documented and understood. This study provides the assessment of soil GHG emissions in the Sudanian savanna region of West Africa using a chamber-based experimental setup. The measurements are taken at four sites with contrasting land use and land management practices: pristine savanna forest, cropland, degraded grassland, and a rainfed rice field. Over two consecutive years (2023–2024) of weekly chamber measurements during the rainy season (corresponding to the rice-growing period), our results reveal significant variation in methane (CH_4) fluxes across the sites. However, nitrous oxide (N_2O) fluxes did not vary significantly, likely due to uniformly low nitrogen input across all systems. The highest seasonal CH_4 emissions were recorded in the rainfed rice field (0.69 ± 0.17 and 0.82 ± 0.22 kg C ha^{-1} $season^{-1}$, on average), while the forest reserve acted as a net CH_4 sink (− 0.019 ± 0.20 and − 0.42 ± 0.13 kg C ha^{-1} $season^{-1}$). In contrast, soils across all sites, both managed and natural, were sources of N_2O, with fluxes ranging from 0.01 kg N ha^{-1} $season^{-1}$ in the forest reserve to 0.16 kg N ha^{-1} $season^{-1}$ in the rice field. This study also analyzed the environmental drivers of GHG fluxes and found that CH_4 variability was significantly influenced by soil water content and soil temperature (partial R^2 between 0.21 and 0.42). No significant relationship was observed between these variables and N_2O emissions. These results highlight that land cover degradation in the Sudanian savanna can substantially increase CH_4 emissions, while its impact on N_2O fluxes is marginal but leads to higher CO_2-equivalent.

Keywords CH_4 flux, N_2O emission, Chamber measurements, Land use, Sudanian savanna, West Africa

Human activities such as land use and land management have led to a steady increase in the atmospheric concentration of major greenhouse gases including N_2O and CH_4 over recent decades, raising concerns about global warming[1–3]. Both N_2O and CH_4 are mainly of biogenic origin, but their monitoring remains limited especially in West Africa. With a global warming potential of 25 times greater than carbon dioxide and a lifespan of less than a decade[1], the atmospheric CH_4 concentration has increased by 161% from 720 ppb in the pre-industrial era to 1879 ppb[4] today. Although CH_4 emissions from agriculture, livestock breeding, and

[1]West African Science Service Center on Climate Change and Adapted Land-Use (WASCAL), Department of Meteorology and Climate Science, Federal University of Technology Akure, Akure, Nigeria. [2]Laboratoire d'Hydrologie Appliquée, Institut National de l'Eau (INE), Université d'Abomey-Calavi, Cotonou, Benin. [3]Institute of Geography, University of Augsburg, Augsburg, Germany. [4]Institute for Meteorology and Climate Research, Karlsruhe Institute of Technology, Atmospheric Environmental Research (IMK-IFU), Garmisch- Partenkirchen, Germany. [5]West African Science Service Centre on Climate Change and Adapted Land Use, WASCAL Competence Centre, Ouagadougou, Burkina Faso. [6]Department of Meteorology and Climate Science, Kwame Nkrumah University of Science and Technology, Kumasi, Ghana. [7]Department of Earth & Environmental Sciences, Michigan State University, East Lansing, MI 48824, USA. [8]Department of Applied Geology, Federal University of Technology Akure, Akure, Nigeria. [9]Center for Climate Resilience, University of Augsburg, Augsburg, Germany. ✉email: francisoussou@gmail.com; harald.kunstmann@kit.edu

manure management[5] are widely reported, the contribution from rainfed farming in West Africa still needs to be thoroughly investigated. The biological and environmental factors that affect CH_4 emissions are manifold[6], but soil moisture regulating soil aeration and thus the balance between methanogenesis and methane oxidation remain one of the most important factors[7].

The atmospheric N_2O concentration has increased by 23.3% from the pre-industrial era to the last decade (0.333 ppm[4], and this is likely to increase[8]. N_2O emission in a particular ecosystem is governed by the microbial processes of nitrification and denitrification in the soil, which in turn are controlled by the soil temperature and moisture[9,10]. The crops' yield improvement with chemical and organic fertilizers has been demonstrated to make a substantial difference between a natural ecosystem and agricultural systems' N_2O emissions[8,11]. Otherwise, in a nearly anaerobic condition, where the end product of denitrification is primarily N_2, the soil can occasionally behave as a N_2O sink[12]. The biological nitrogen fixation (BNF) of atmospheric N_2 by the leguminous crops is a potential way to reduce N_2O emissions[13]. N_2O fluxes under legume-based agroecosystems are reported to be relatively low compared to other generally cultivated crops even during pre-crop cultivation[14–16]. However, the combined effect of pedoclimatic and fertilization practices is a rather complex driver of N_2O fluxes[17,18]. Due to the high temporal dynamic of the N_2O fluxes, it is recommended that N_2O emissions be monitored continuously at a relatively high temporal resolution[19]. In case of a rapidly changing land cover in West Africa[20,21], the monitoring of GHG emissions of different land use and management conditions is highly required for both mitigation and adaptation purposes[22]. The N demand for plant growth in grassland systems has a significant impact on N_2O emissions[23]. However, the overall impact of changes in land use and management on the emission of N_2O remains uncertain, as this depends on various factors, such as the type of ecosystem, local climatic conditions, and land management practices[24,25].

Soil temperature and moisture levels controls the oxygen availability in the soil matrix[24]. Microbial activities that control the biogenic release of N trace gases include nitrification and denitrification[26]. The ammonium NH_4^+ in the soil is formed through the mineralization of organic material and this constitutes the substrate needed for autotrophic and heterotrophic nitrification. The oxidation of NH_4^+ to nitrate (NO_3^-) occurs through hydroxylamine (NH_2OH) and nitrite (NO_2) in aerobic conditions by nitrifying organisms. Denitrification in opposite occurs in anaerobic conditions where NO_3^- and NO_2 serve as electron acceptors. Through nitric oxide (NO), NO_2, and N_2O, the NO_3^- can be reduced to inert nitrogen (N_2). The balance between nitrification and denitrification rates controls the N_2O and NO emissions from soil in response to peculiar environmental conditions. The gas diffusion and metabolic activity in the soil are controlled by the heterogeneity of the soil as direct effects of the soil aeration status. This defines to what extent nitrification and denitrification will occur[9,27]. Previous studies[28,29] reported that the magnitude of N_2O emission in tropical soils is mainly driven by the aeration status and soil pH. The strong rainfall seasonality in African savannas influences the soil aeration status as demonstrated by Andersson et al. (2003)[30].

The global efforts for climate change adaptation and mitigation are mainly focused on carbon dioxide emissions. However, the global warming potential (GWP) of nitrous oxide (N_2O) is 265 times higher with life span over a century[4,31]. The highest rate of total N_2O emissions due to human activities comes from the agricultural sector[32,33]. N_2O emissions from agricultural soils are direct consequences of animal excreta and fertilizer applications[34]. The needs for organic nitrogen fertilizers can range from improving crop yield to intensive grass growth simulation for large scale grazing events[35]. Two types of nitrogen (N) spreading responsible for increased N_2O losses are the cumulative effects of fertilizers application on top of animal excreta and on urine and dung deposits[36–39]. The ratio of N_2O release to uptake is therefore further exacerbated at the affected spots when both the plant N demand and soil microclimatic conditions tilt the balance in the emission direction[40]. Notwithstanding the aforementioned evidence, further investigations in poorly documented regions are necessary for an improved process understanding and for making better decisions when managing agricultural systems in these areas.

The overarching goal of this study is to investigate the N_2O and CH_4 emissions in dominant land use systems of the Sudanian savanna of West Africa. Measurements were carried out at four eddy covariance flux tower sites selected to represent typical land use and management practices in this region: (1) a protected savanna woodland within a national forest reserve, (2) a rainfed paddy rice field, (3) semi-degraded grassland, and (4) a mixed-use rainfed cropland system[2,41–43]. Thus, the study assesses for the first time the N_2O and CH_4 emissions from rainfed rice fields in parallel to a reference site (forest reserve) and two other important land use practices (grassland and cropland) in this region. Based on this experimental setup, the study aims to address three key research questions: (1) How do CH_4 and N_2O emissions vary across different types of land use in the Sudanian savanna of West Africa? (2) How do these emissions compare with those reported in previous chamber-based studies conducted in the region? and (3) What are the primary environmental drivers regulating CH_4 and N_2O fluxes across these systems?

Materials and methods

Study region and sites description

This study was undertaken at four contrasting greenhouse gases monitoring locations in the Sudanian savanna, Northern Region, Ghana for two consecutive rainy seasons (2023 and 2024; see Fig. 1). The land use types are cropland (Kayoro), semi-degraded grassland (Gorigo), rainfed paddy rice fields (Janga) and a protected savanna woodland within a national forest reserve (Mole Park). The monitoring locations are part of the WASCAL-hydrometeorological observatory installed in the last decade[2,40,41]. This region is heavily utilized for agricultural purposes. The natural savanna vegetation was therefore strongly converted to different agricultural systems in this region over the past decades water, energy and carbon fluxes at the different sites are monitored with the Eddy Covariance method[2,42–44] since 2013 at Kayoro, 2017 at Gorigo, 2022 at Janga, and 2023 at Mole Park.

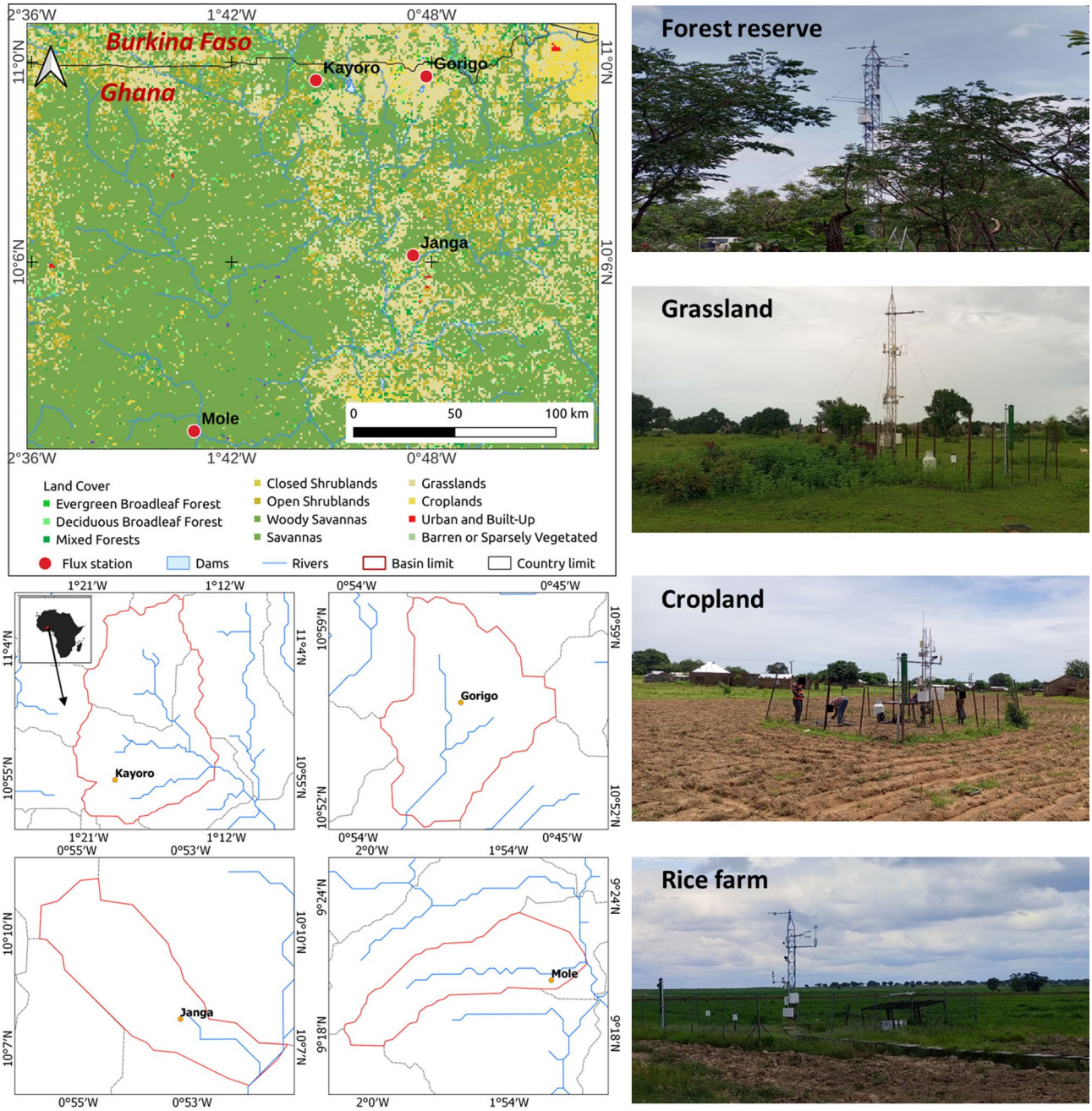

Fig. 1. Study region and the four monitoring sites Kayoro "cropland", Gorigo "grassland", Janga "rice fields" and Mole Park "forest reserve". The five maps are produced with the freely available QGIS software version 3.10.9 (https://download.qgis.org) and the 4 pictures are from the field campaign of 2023 and 2024.

In addition, chamber measurements were taken at these sites in 2023 and 2024 to further ascertain the N_2O andCH_4 fluxes (Fig. 2).

The geographic boundaries of the area extend from latitude 9°26.4'N to 11°12.4'N and longitude 2°12'W to 0°.41.4'W with the altitude varying from 93 to 488 m. The seasonal cycle of rainfall is strongly linked to the movement of the rainfall belt of the West African Monsoon determining the rainfall onset and cessation[45,46]. The annual rainfall is monomodal in the southern Sudanian savanna extending between May and October. The mean annual precipitation ranges between 900 mm and 1100 mm[41,47]. The annual average air soil temperature varies between 26 and 33 °C. Different dominant vegetation species are reported in the area, such as *Lannea microcarpa* (Wild grape), *Adansonia* (Baobab), and *Parkia biglobosa* (Néré tree)[43]. Near the flux tower, the cultivated crops in 2023 and 2024 are soybean and groundnut at the cropland site (Kayoro). Further site characteristics about Kayoro and Gorigo are given by Bliefernicht et al. (2018)[41], and Mole Park and Janga in Guug et al. (2025)[2]. During the gas sampling period, the cropland was ploughed and fertilized after applying a selective herbicide (Glyphosate 410 g/L SL) on the 18th July 2023 and 24th June 2024 at the cropland site. Likewise, the rice fields

Fig. 2. Chamber-based greenhouse gas sampling plots; closed (middle) and opened for soil moisture and soil temperature measurements (left and right) in a rice field at Janga, Upper-East Ghana.

were subjected to similar agricultural practices on the 25th July 2023 and 26th June 2024. The local community undertook a low-intensity mixed grazing of livestock (cattle and sheep) at the grassland site.

Procedures of the field GHG measurement

Experimental design

The field campaign with the chamber measurements was done in 2023 and 2024 on a weekly basis covering the peak monsoon period and therefore the main vegetation and cultivation period in this region (Fig. 2). First samples were collected at Kayoro, Gorigo and Janga by the end of May 2023 (29th of May 2023). Sampling at the Mole Park started end of July 2023. The sampling was done in the morning, between 9 and 11 AM, when the turbulent fluxes of the planetary boundary layer deploy progressively until the highest around the noon time. Because of this time constraint and the average distance (105 ± 50 km) to the EC sites, the gas sampling is undertaken for each site per day. The sampling is done at Gorigo, Kayoro, and Janga from Monday to Wednesday and the Mole Park gas sample is collected later during the week.

The chamber-based measurement of greenhouse gases deployed in this study is similar to the experimental design used in various ecosystems in the last decades[19,34]. In this study, the designed chamber is made of two parts: the collar and the intransparent lid. It is a 37 × 26.7 cm size collar which is implanted at 10 m from the EC tower. Five sub-trial points (chambers) are deployed at each site to ascertain the spatial variability. The first is located at the north (0 N) and the following at an interval of 72 degrees.

Chamber sampling and analysis

De Klein & Harvey (2015)[48] described a static chamber method for the N_2O measurements. In this study, a chamber collar was inserted into the ground at 2–5 centimeters depth and left on the field throughout the measurement periods. The average head space volume is approximately 20 L. The sampling started with the soil moisture and soil temperature measurements for each sub-trial chamber. For 20 min, the chambers are closed and the gas sample is taken at 5, 10, 15 and 20 min at the top of the chamber through a rubber septum. A 50 mL poly-propylene syringe attached to a hypodermic needle is used to extract the air from the closed chamber. The gas sample is then transferred into a sealed and pre-evacuated glass exetainer of 10 mL (SRI Instruments, Bad Honnef, Germany). The choice of the sampling period (9:00 to 11:00 AM) is based on the suggestions that 94 to 101% of the "true" seasonal emissions is captured early in the morning and evening[49,50]. The sampling is undertaken every week almost the same day of the week for each site. During the sampling, 50 ml of gas is taken from the chamber using a syringe. 70% of the sample is used to flush the empty vial, after which the remaining 15 mL is injected with a slight overpressure in the 10 mL vial[51].

At the end of the sampling process, the chambers' height, soil moisture, and soil temperature are measured. The gas samples were packaged and sent to the KIT, IMK-IFU (Garmisch-Partenkirchen, Germany). The gas chromatograph (8610 C; SRI Instruments, Torrence, USA) used to measure the gas concentration in the samples is equipped with an auto sampler (HT200H; HTA s.r.l, Brescia, Italy), an electron capture detector (ECD N_2O), and a flame ionization detector/methanizer (FID: CH_4 and CO_2). Further, the concentrations of the standard gas that served for the sample calibration are 400 (396 ± 40) ppb for N_2O and 4000 (4113 ± 82) ppb for CH_4 (Air Liquide, Düsseldorf, Germany). Following the approach used in Parkin, Venterea, and Hargreaves[52], the mean detection limits were computed and resulted in 4.40 µg CH_4-C and 0.68 µg N_2O–N m^{-2} hr^{-1}. The gas fluxes are computed as follows:

$$F_{CH} = \frac{d_q}{d_t} \times \frac{V \times P \times M_w}{R \times T} \times \frac{60}{A \times 1000} \quad (1)$$

$\frac{d_q}{d_t}$: change in the mixing ratio over time (ppb min^{-1} or ppm min^{-1}) resulting from the linear fit, T: average soil temperature during sampling (°K), P: long-term average air pressure of the site (Pa), V: chamber volume (m^3), Mw = 12 for CH_4 and Mw = 28 for N_2O (g mol − 1), A is the surface area of the chamber (m^2) and R is the universal gas constant (J mol^{-1} $°K^{-1}$).

Two main criteria are followed to calculate the monthly means for each land use after the quality control. In case the calculated flux is an outlier, the estimated flux is benchmarked against the temporal average from previous values, and a measurement is considered valid if the coefficient of determination is greater than 0.8, 0.6, and 0.6, respectively for CO_2, CH_4, and N_2O fluxes. If the coefficient is less than 0.8 for the CO_2 flux, the calculated fluxes for the site that week are altogether rejected. The fluxes are valid if the coefficient is greater than 0.8 for CO_2 flux and 0.6 for N_2O and CH_4 fluxes[50]. The cumulative GHG fluxes were also computed for each gas by linearly interpolating fluxes between sampling dates and integrating the interpolated time series using the trapezoidal rule. This approach accounts for irregular temporal sampling and avoids bias associated with arithmetic averaging. Cumulative emissions were converted to kg ha^{-1} $season^{-1}$, and CO_2-equivalent emissions were calculated using 100-year global warming potentials from IPCC Sixth Assessment Report (AR6). The constants are 27.2 and 273.0 for CH_4 and N_2O, respectively. Uncertainty was quantified using non-parametric bootstrap confidence intervals with a 95% confidence interval (CI).

Soil moisture and soil temperature measurements

Each gas sampling procedure is preceded by the soil volumetric water content (VWC) and temperature measurement. The soil thermometer and moisture sensor are implanted inside the chamber collar and the values are read on the device screen. Following the recommendation of Werner et al.[25], the soil water-filled pore space (WFPS) is calculated using VWC values.

Soil sampling and analysis

Before the GHG sampling, soil core samples are collected at 5 different depths (0–5 cm, 5–10 cm, 15–20 cm, 30–35 cm, 45–50 cm) with four soil profiles per depth at each site (Table S2). The soil physicochemical properties were measured at Janga, Kayoro, and Gorigo (n = 45). The samples are dried at low temperature (~ 40 °C) and sieved with a 5 mm sieve. They are properly kept in plastic and transported to the KIT IMK-IFU laboratory (Germany), where the nitrogen content and soil organic carbon are measured. The bulk density (BD) is also calculated for each soil sample dried at 105°C for 24h[53]. The soil volumetric water content and BD values are used to calculate the soil water filled pore space (WFPS) following the suggestions of Werner et al.[25].

$$WFPS\,[\%] = \frac{W_{vol}}{\left(1 - \frac{BD}{2.65}\right)} \quad (2)$$

$W_{vol}$is the volumetric water content, BD the bulk density [$g\ cm^{-3}$], and 2.65 the particle density [$g\ cm^{-3}$].

The isotopic signature of carbon ($\delta^{13}C$) and nitrogen ($\delta^{15}N$) of each sample is also measured. The isotope Ratio Mass Spectrometry test AIL-1.1c (2015-02) used for the analysis is a flexibly accredited method by the European standard DIN EN ISO/IEC 17025:2018 which was released in February 2015. The analysis of the ratios of the stable carbon isotope $\delta^{13}C/\delta^{12}C$ shows altogether a higher rate of $\delta^{12}C$ at the three managed sites originating from a mixture of C3 and C4 plants with dominance towards C4 (Fig. S1). For all the sites, the ratios oscillate from − 19.9 to −14.3‰ with respectively an average of −17.29 ± 0.1, −17.93 ± 0.11, and − 17.48 ± 0.1 for the grassland, cropland, and rice fields. Similar ranges between − 24 and − 13‰ at a grassland, −18 and − 15‰ at a maize field, and − 17 and − 15‰ are obtained by Gerschlauer et al.[54] at Kilimanjaro mount. The carbon ratio increases slightly with the depth at the grassland and cropland sites while the values remain in the same range at the rice fields. Unlike the low nitrogen content, the carbon content is relatively moderate to low with $\delta^{13}C$ averages of 0.23 ± 0.0%, 0.23 ± 0.1%, and 0.47 ± 0.2% respectively.

Statistical analysis

The sampling period extends from May to October for the two consecutive years. Annual and monthly means are calculated for each year. Kolmogorov-Smirnov test is used to evaluate the normality of the variables. The repeated-measures ANOVA test is used to assess the difference in average flux between the 4 sites for the same period. For the difference between the two years, the paired t-test is used as the fluxes are paired by week (e.g., week 21 of 2023 compared with week 21 of 2024). The environmental controls over the GHG fluxes at each site are evaluated using the multiple stepwise regression analysis. The factors considered are WFPS and soil temperature.

Results

Methane emissions

This study assessed for the first time rainfed rice fields methane emissions in the Sudanian savanna using the chamber-based approach. The fluxes oscillate from − 33.08 to 13.72 µg C m^{-2} h^{-1} in 2023 and − 33.8 to 29.13 µg C m^{-2} h^{-1} in 2024 with seasonal median of −13.86 µg C m^{-2} h^{-1} at Mole Park (Table 1). The forests site acts as a CH_4 sink as the averages of the seasonal fluxes are − 0.52 and − 11.48 µg C m^{-2} h^{-1} for 2023 and 2024. The lowest value was recorded in July 2024 while the strongest flux occurred in September 2024. Throughout the season, the grassland remains predominantly a CH_4 source with fluxes varying from − 24.13 to 73.58 µg C m^{-2} h^{-1} in 2023

Site name	Land cover	Altitude (m)	AP (mm)		MAT (°C)		$\delta^{13}C/\delta^{12}C$ (‰)	Soil C (%)	Ntot (%)	C/*N*	Nr	BD (g/cm^3)	Texture (%) sand/silt/clay	Soil types
			2023	2024	2023	2024								
Mole	Forest	159	1029*	889*	28.36*	28.63*	–	1.62 ± 0.35	0.154 ± 0.03	10.64	–	–	–	
Gorigo	Grassland	217	952*	1042*	28.97**	32.55**	− 17.29 ± 0.1	0.32 ± 0.015	0.04 ± 0.0	8	–	1.66 ± 0.11	–	
Kayoro	Cropland	292	959*	877.9**	29.99**	29.57**	− 17.93 ± 0.1	0.39 ± 0.11	0.046 ± 0.012	8.48	Low	1.65 ± 0.08	770.9/20.05/2.87	Loamy sandy
Janga	Rice fields	118	883*	1011*	26.05**	26.52**	− 17.48 ± 0.1	0.62 ± 0.092	0.057 ± 0.005	10.88	Low	1.53 ± 0.09	–	

Table 1. Descriptions of the investigated sites: altitude, annual precipitation (AP), mean annual air temperature (MAT), soil organic carbon (SOC), soil nitrogen (Ntot), soil carbon to nitrogen ratio (C/N), N fertilization rate (Nr), bulk density (BD), texture (%), and soil types. The parameters refer to soil depth from 0 to 50 cm. The values are derived from eddy covariance measurements (**) and reanalysis products (*) because of missing data. Further details about the sites are provided in Quansah et al. (2015), Bliefernicht et al. (2018), and Berger et al. (2019).

and −16.15 to 64.25 µg C m^{-2} h^{-1} in 2024. The seasonal average and median are 14.44 and 13.49 µg C m^{-2} h^{-1} for 2023 and 10.13 and 8.04 µg C m^{-2} h^{-1} for 2024, respectively. At the cropland site, the perturbed soil resulted in a CH_4 sink with an average of −1.78 and −2.05 for the two years with seasonal medians of −4.79 and −3.45 µg C m^{-2} h^{-1}. The maximum fluxes show a glimpse of the warming potential of the four ecosystems (Table 2). The Rice fields CH_4 release reaches 8 to 15-folds the forest reserve and cropland maximum fluxes while the grassland shows approximately 2 to 6-folds. Further, the CH_4 sink potential is demonstrated in the minimum fluxes as for the two consecutive years, the forest reserve maintained the highest sink followed by the cropland, the grassland, and the Rice fields (see Table 2). However, a CH_4 sink of −40.18 µg C m^{-2} h^{-1} was recorded in the Rice fields on the 28th August 2024 under moderate soil temperature (34.35 °C) and soil moisture of 42.26%WFPS. The highest seasonal mean of CH_4 emission in 2023 and 2024 occurred in the rice fields (0.69 ± 0.17 kg C ha^{-1} $season^{-1}$ and 0.82 ± 0.22 kg C ha^{-1} $season^{-1}$ - Fig. 3).

The repeated-measures ANOVA indicate a significant difference ($p < 0.05$) in methane emissions between the four land-use conditions. Except for the forest reserve, there is no significant difference among the years. Compared to other sites, the methane sink in the Forest reserve is significantly higher with the highest value recorded in June 2024 (−25.41 µg C m^{-2} h^{-1}). The second highest emission occurs in the grassland (0.53±0.35 kg C ha^{-1} $season^{-1}$ and 0.37±0.13 kg C ha^{-1} $season^{-1}$) while the most significant methane sink is recorded in the Forest reserve (−0.019±0.2 kg C ha^{-1} $season^{-1}$ and −0.42±0.13 kg C ha^{-1} $season^{-1}$). The emission is low in the cropland (−0.065±0.2 kg C ha^{-1} $season^{-1}$ and −0.074±0.14 kg C ha^{-1} $season^{-1}$) where the soil is disturbed by agricultural practices at the beginning of the growing season. During the rainfall onset in June, the grassland behaves as a net CH_4 release (4.26±14.3 and 5.33±5.0) for the two years while the forest reserve indicates the highest sink (−25.41±4.8 µg C m^{-2} h^{-1}) in 2024. The soil at the cropland site absorbs 7.18±6.2 µg C m^{-2} h^{-1} and 0.5±7.0 µg C m^{-2} h^{-1} CH_4 in the same period (Table 2; Fig. 3). The rainfall onset delay at the rice fields in 2024 is revealed in the measurement as the soil indicates a CH_4 sink of −6.19±15.3 µg C m^{-2} h^{-1} while the previous year was a release of 4.96±16.8 µg C m^{-2} h^{-1}.

In July, except for the CH_4 sink at the forest reserve (−19.93 ± 5.9) in 2024, the average CH_4 release was 6.44 ± 11.18 µg C m^{-2} h^{-1} and 3.31 ± 0.9 µg C m^{-2} h^{-1} at the grassland, 0.77 ± 8.7 µg C m^{-2} h^{-1} and 0.70 ± 5.0 µg C m^{-2} h^{-1} at the cropland, and 16.90 ± 15.8 µg C m^{-2} h^{-1} and 1.89 ± 11.3 µg C m^{-2} h^{-1} at the rice fields (see Table S1). The methane sink observed in the previous month continued in August in the forest reserve, with a sink of −3.24 and −16.98 µg C m^{-2} h^{-1} for the two years. In contrast, the methane release is maintained in the grassland and cropland. Though a similar pattern is observed at the rice fields in 2023 (40.89 µg C m^{-2} h^{-1}), dry spells during the rainy season of 2024 (31.19% WFPS) in the sampling period is accompanied by methane sink (−8.05 µg C m^{-2} h^{-1}), which is unlikely for the period and site. Toward the end of the growing season, the

		Seasonal mean [µg C/*N* m^{-2} h^{-1}]		Min [µg C/*N* m^{-2} h^{-1}]		Max [µg C/*N* m^{-2} h^{-1}]		Median [µg C/*N* m^{-2} h^{-1}]		ΣMin [kg C/*N* ha^{-1} $season^{-1}$]		ΣMax [kg C/*N* ha^{-1} $season^{-1}$]		ΣMedian [kg C/*N* ha^{-1} $season^{-1}$]	
	Ecosystem	2023	2024	2023	2024	2023	2024	2023	2024	2023	2024	2023	2024	2023	2024
CH_4	Forest	− 0.019 ± 0.2	− 0.42 ± 0.13	− 33.08	− 33.8	13.72	29.13	4.92	− 13.86	− 0.46	− 0.45	0.13	− 0.11	− 0.26	− 0.35
	Grassland	0.53 ± 0.35	0.37 ± 0.13	− 24.13	− 16.15	73.58	64.25	13.49	8.04	0.20	0.05	0.69	0.55	0.57	0.33
	Cropland	− 0.065 ± 0.2	− 0.074 ± 0.14	− 27.46	− 17.35	18.13	15.56	− 4.79	− 3.45	− 0.31	− 0.25	0.04	0.06	− 0.05	− 0.01
	Rice fields	0.69 ± 0.17	0.82 ± 0.22	− 17.23	− 40.18	140.07	233.9	14.6	5.47	0.28	− 0.11	0.86	0.59	0.38	0.54
N_2O	Forest	0.12 ± 0.1	0.011 ± 0.11	− 9.31	− 10.56	12.1	9.27	6.32	− 1.37	− 0.01	− 0.11	0.11	0.13	0.03	− 0.02
	Grassland	0.05 ± 0.16	0.1 ± 0.02	− 13.21	− 9.65	14.14	21	3.3	3.25	− 0.07	− 0.01	0.31	0.13	0.06	0.12
	Cropland	0.12 ± 0.18	0.1 ± 0.08	− 12.18	− 15.84	16.51	29.63	6.11	2.55	− 0.09	− 0.13	0.18	0.34	0.15	0.07
	Rice fields	0.08 ± 0.24	0.16 ± 0.31	− 9.74	− 11.09	12.59	33.93	3.65	4.66	− 0.03	0.09	0.13	0.20	0.06	0.16
SM [%]	Forest	16.59 ± 4.3	10.55 ± 0.0	7.9	10.55	23.55	10.55	18.1	10.55	7.9	10.55	23.55	10.55	18.1	10.55
	Grassland	19.78 ± 8.95	18.61 ± 8.02	0.1	4.3	40.15	33.95	19.45	17.13	0.1	4.3	40.15	33.95	19.45	17.125
	Cropland	11.97 ± 5.29	10.56 ± 6.01	0.5	0.3	22.3	21.25	12.85	11.25	0.5	0.3	22.3	21.25	12.85	11.25
	Rice fields	25.41 ± 11.7	17.18 ± 10.5	0.5	5.35	39.15	36.15	31.6	14.25	0.5	5.35	39.15	36.15	31.6	14.25
T_{soil} [°C]	Forest	28.43 ± 0.46	28.3 ± 0.0	26.45	26.45	31.05	30.15	27.82	27.87	26.45	26.45	31.05	30.15	27.82	27.87
	Grassland	29.81 ± 1.48	31.26 ± 2.86	26.75	28.5	32.35	40.9	29.92	30.25	26.75	28.5	32.35	40.9	29.92	30.25
	Cropland	29.19 ± 2.91	31.41 ± 2.78	24.8	27.65	34.5	37.75	28.5	31.22	24.8	27.65	34.5	37.75	28.5	31.22
	Rice fields	30.78 ± 2.34	31.42 ± 2.51	27.75	26.95	36.25	34.75	30.25	32	27.75	26.95	36.25	34.75	30.25	32
WFPS [%]	Forest	–	–	–	–	–	–	–	–	–	–	–	–	–	–
	Grassland	53.05 ± 24.0	49.9 ± 21.5	0.26	11.52	107.65	91.02	52.15	45.91	0.26	11.52	107.65	91.02	52.15	45.91
	Cropland	32.11 ± 4.48	28.33 ± 16.2	1.32	0.79	59.27	56.48	34.15	29.9	1.32	0.79	59.27	56.48	34.15	29.9
	Rice fields	59.99 ± 27.6	40.56 ± 24.9	1.18	12.63	92.42	85.34	74.6	33.64	1.18	12.63	92.42	85.34	74.6	33.64

Table 2. Descriptive statistics of the seasonal N_2O and CH_4 fluxes, soil temperature (T_{soil}), water filled pore space (WFPS) of the four sites for the two years. The values are in kg C/N ha^{-1} $season^{-1}$ for the minimum, maximum, median and cumulative fluxes while the monthly averages and seasonal mean are reported in µg C m^{-2} h^{-1} (see table S1). The period of the season considered for the seasonal mean and cumulative fluxes computation is from June to October.

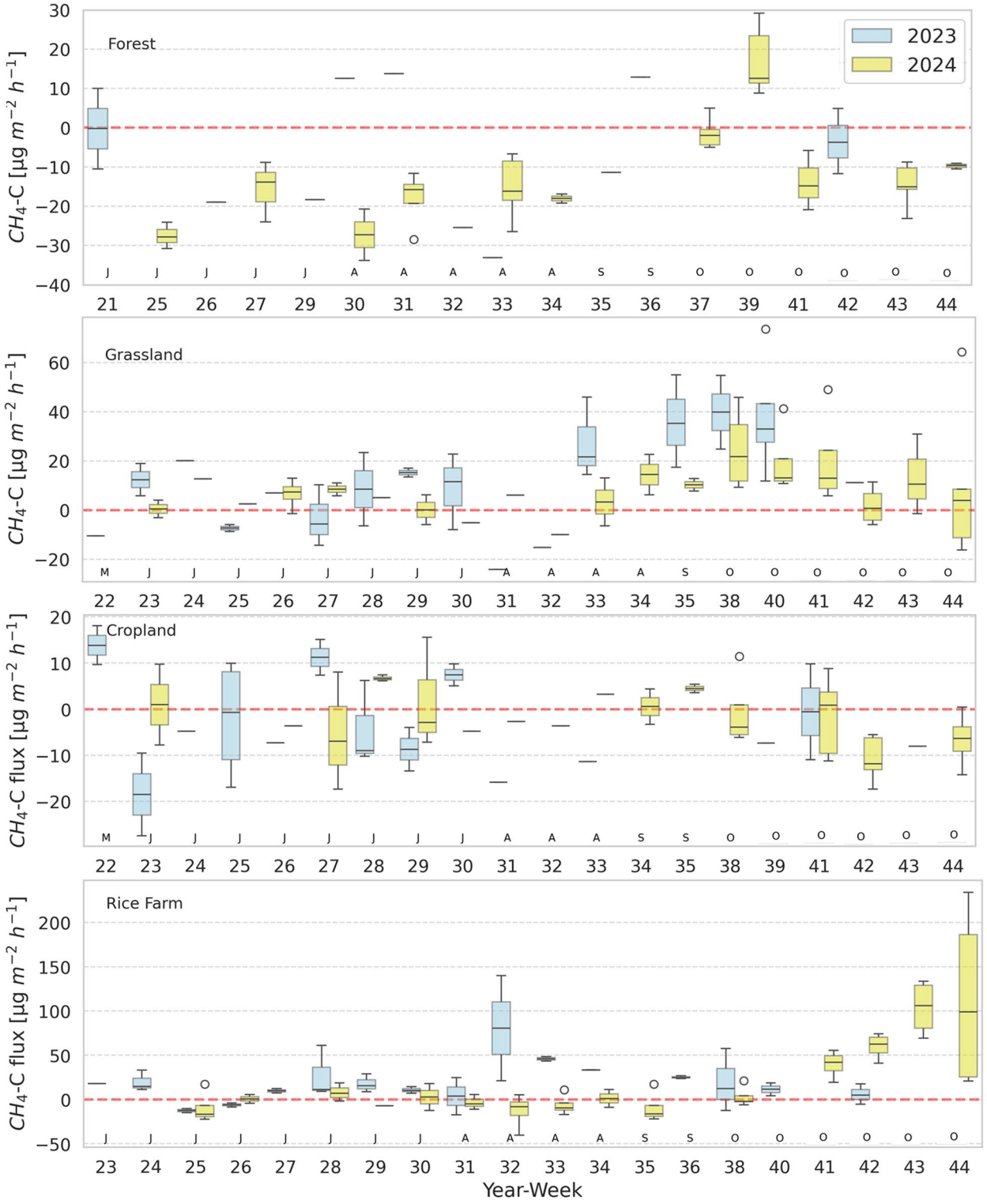

Fig. 3. Weekly boxplot time series of in situ CH_4 flux for 2023 (light blue) and 2024 (yellow). Each boxplot is made of fluxes from 5 sub-trial points (chambers). From top to bottom are the forest reserve, grassland, cropland, and rice fields. The number of the sampling week is in x-axis.

forest reserve switched to methane release (12.91 and 7.84 µg C m^{-2} h^{-1}) in September. Likewise, the cropland methane release in the previous month changed to sink (−7.34 and − 0.64 µg C m^{-2} h^{-1}). The magnitude of the CH_4 flux rate at the grassland site increased significantly by 2 to 3 folds while it decreased at the rice fields. In October, the emissions at the forest reserve changed back to CH_4 sink (−3.48 and − 12.75 µg C m^{-2} h^{-1}). The CH_4 release was maintained at the grassland (32.53 and 12.77 µg C m^{-2} h^{-1}) and rice fields (8.03 and 79.16 µg

C m^{-2} h^{-1}) while the cropland shows a methane sink (−0.57 and − 6.4 µg C m^{-2} h^{-1}). Overall, the temporal pattern indicates a rise in the emission in response to the rainfall at each site. The magnitude of emission is lower at the beginning of the rainy season while the highest release is reached at the peak (July-August). This is followed by a decrease of the emission towards rainfall cessation. There is a remarkable difference between the cropland and rice fields' emissions. The soil disturbance (e.g., ploughing) reduces the ability of the bacteria to produce methane. A stable soil structure is required for increased methane release. The cropland methane flux is mitigated with wetter and drier soil conditions resulting respectively in emission and uptake. The methane flux in the rainfed rice (Janga) is significant compared to other land use however compared to permanently flooded rice fields (0.2 to 99 mg C m^{-2} h^{-1})[55], the values are quite lower (see Table 2). Hence, this lower methane emission in the rainfed rice is further confirmed in the earlier weeks of the rainy season when the soil behaves as a sink (−6.19 ± 15.3) in 2024 and slight release (4.96 ± 16.8) in 2023.

The dominant role of rainfall variability and biogeochemical controls on methane production and oxidation is shown in Fig. 4a as it reveals strong land-use dependent contrasts in cumulative CH_4 fluxes over the rainy season. A negative cumulative flux is observed at the Forest site (−0.52 kg C ha^{-1} $season^{-1}$ and − 0.35 kg C ha^{-1} $season^{-1}$) for both years and most of the chambers consistently acted as a net CH_4 sink throughout the season. This characterizes a well-aerated upland soils where methanotrophic oxidation exceeds methanogenesis, and

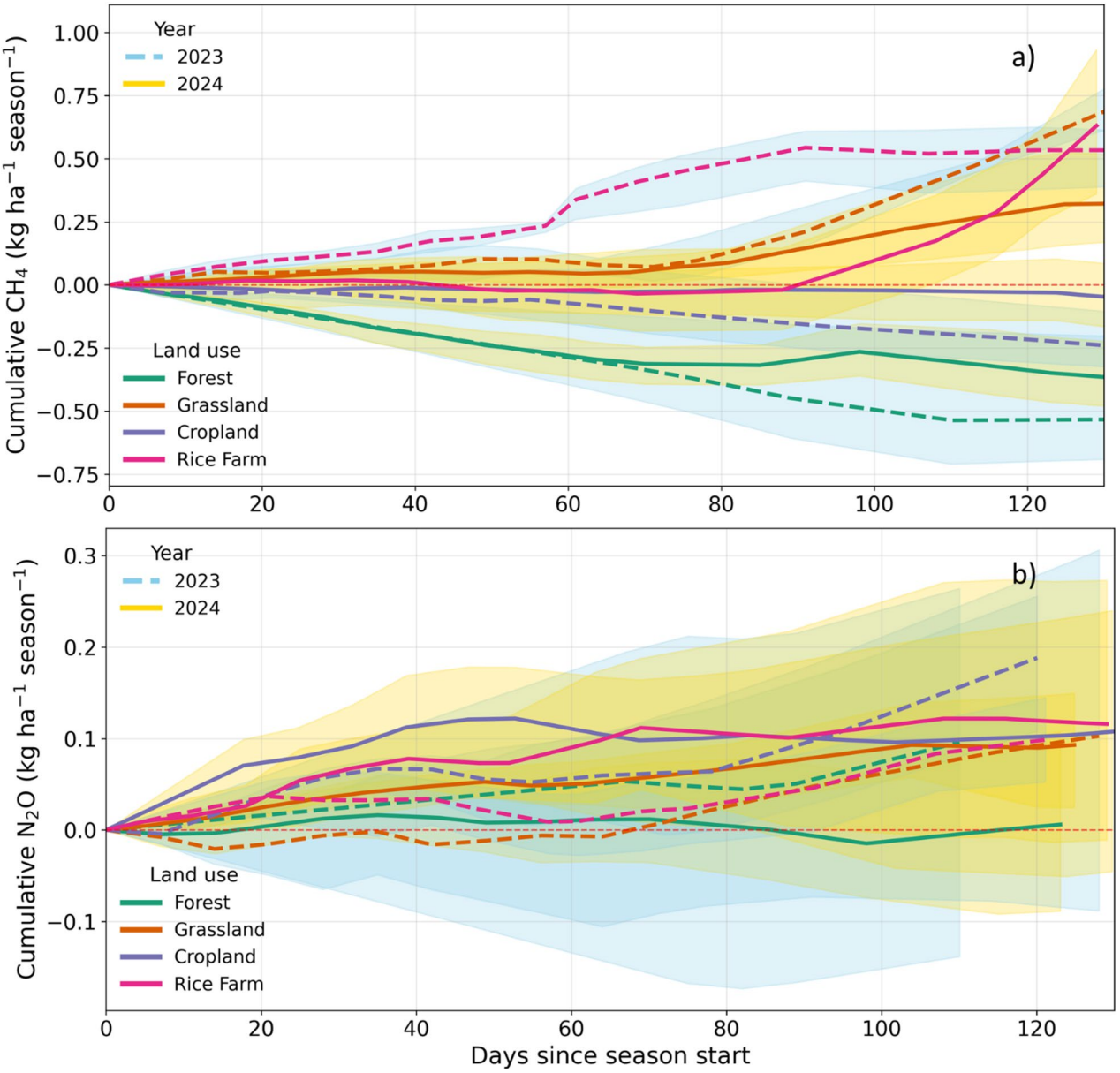

Fig. 4. Cumulative CH_4 (**a**) and N_2O (**b**) fluxes from the investigated land use covering the rainy season. The dashed lines represent 2023, and the solid lines represent 2024. Thicker lines indicate the seasonal average from the 5 chambers with corresponding confidence intervals (95% CI) in blue and yellow for 2023 and 2024, respectively. The global warming potential (kg CO_2-eq) of the fluxes is shown in Fig. S3a-b.

the relatively narrow confidence intervals in 2024 show a robust and spatially consistent sink across chambers. However, near-neutral to weakly negative cumulative CH_4 flux is recorded at the cropland site (−0.07 and − 0.18 kg C ha^{-1} $season^{-1}$) despite the spatial disparities among the chambers. Grassland system exhibited near-neutral to weakly positive cumulative CH_4 flux before ~ 70th day but spiked strongly later reaching 0.38 and 0.64 kg C ha^{-1} $season^{-1}$ varying substantially towards the end of the season. This suggests a temporal suppression of CH_4 oxidation in response to accumulated rainfall and increased soil moisture, a transition toward more reducing soil conditions. Croplands highlighted the highest intra-seasonal and spatial heterogeneity among the chambers, varying between small net uptake and emission phases, likely revealing transient soil moisture conditions and management-induced heterogeneity such as residue inputs or soil disturbance.

In contrast, Rice fields showed pronounced positive cumulative CH_4 emissions in both years, with a clear acceleration during the latter half of the rainy season especially in 2024. In flooded soils, sustained anaerobic conditions occurred promoting methanogenesis via acetoclastic and hydrogenotrophic pathways. Approximately 80–100 days after the season start, the sharp increase highlights a coupling between prolonged inundation, substrate availability, and microbial community establishment. Overall, the land-use gradient from Forest to Rice fields corresponds closely to an increasing prevalence of anaerobic microsites and reduced gas diffusivity, reinforcing the central role of soil redox status in regulating seasonal methane budgets. The difference between individual chamber trajectories and the thicker mean curves further illustrates that, while point-scale variability is substantial particularly in managed systems the ecosystem-scale seasonal signal remains coherent within each land-use type. As shown in Fig. S3 for corresponding CO_2-equivalent, the dominant contributor to landscape-scale greenhouse forcing in the rainy season is the Rice Fields whereas forests consistently offset a portion of CH_4 emissions from agricultural systems.

Nitrous oxide fluxes

In the forest reserve, the N_2O fluxes range from − 9.31 to 12.1 μg N m^{-2} h^{-1} in 2023 and − 10.56 to 9.27 μg N m^{-2} h^{-1} in 2024 with seasonal medians of 6.32 and − 1.37 μg N m^{-2} h^{-1}. Similar range of minimum N_2O sink is recorded in the grassland (−13.21 and − 9.65 μg N m^{-2} h^{-1}) however the maximum release is stronger with N_2O fluxes reaching 14.14 and 21 μg N m^{-2} h^{-1}. The seasonal median flux was 3.3 in 2023 and 3.25 μg N m^{-2} h^{-1} in 2024. Further, the cropland displays the strongest N_2O release in September 2023 (16.51 μg N m^{-2} h^{-1}) and June 2024 (29.63 μg N m^{-2} h^{-1}) however, the highest observed N_2O sinks were − 12.18 and − 15.84 μg N m^{-2} h^{-1} in July and September. Under moderate soil temperature and high soil moisture, the highest N_2O flux occurred in the rice fields (33.93 μg N m^{-2} h^{-1}) while the highest sink was − 11.09 μg N m^{-2} h^{-1} in September. The seasonal medians of the two years are close to the observed fluxes in other land use (3.65 and 4.66 μg N m^{-2} h^{-1}) likewise the minimum N_2O sink (−9.74 and − 11.09 μg N m^{-2} h^{-1}).

The paired t-test revealed no significant difference in mean N_2O flux for each land use between the two years. Likewise, the N_2O emissions in both the natural and degraded land cover have no significant difference between the sites. Whatever the observation sites, the investigated land use is a net source of N_2O for each year (Fig. 5). The lowest annual mean of N_2O release was recorded at the forest reserve in 2024 (0.011 ± 0.11 kg N ha^{-1} $season^{-1}$) however the rice fields displayed the highest values (0.16 ± 0.31 kg N ha^{-1} $seasonr^{-1}$). There is a slight change in the annual mean of N_2O release at the cropland site (0.12 ± 0.18 and 0.11 ± 0.08 kg N ha^{-1} $season^{-1}$) while it increased by approximately 127% in the grassland. During the rainfall onset (June), a significant N_2O release is observed for the two years at the cropland (9.52 and 10.48 μg N m^{-2} h^{-1}) and rice fields (9.76 and 10.15 μg N m^{-2} h^{-1}) sites (Table S1). A contrasting land cover effect on N_2O emissions is observed in 2024 as the forest reserve showed N_2O sink (−1.38 μg N m^{-2} h^{-1}) while the grassland displayed a release of 4.42 μg N m^{-2} h^{-1}. Further, the sites altogether released N_2O in July 2024 with the highest value recorded at the rice fields (8.47 μg N m^{-2} h^{-1}). In July 2023, except for the forest reserve, the other three sites behaved as a sink. The rainfall peak in August at the natural forest reserve results in N_2O sink for 2023 (−0.5 μg N m^{-2} h^{-1}) and 2024 (−0.5 μg N m^{-2} h^{-1}). The opposite occurred at the grassland site (4.36 and 3.57 μg N m^{-2} h^{-1}) and even higher flux was observed at the rice fields (6.71 μg N m^{-2} h^{-1}) in 2024. Though there is no significant difference in mean N_2O among the sites, the N_2O release during the rainfall cessation at the forest reserve and grassland is the highest (6.88 and 5.42 μg N m^{-2} h^{-1}) in 2023 (Table S1). The managed systems (cropland and rice fields) showed lower N_2O release compared to the natural systems (Forest reserve and grassland) for the two years in the same period. Lower nitrogen content in response to plant activities at the end of the growing season might explain the lower emission. The evidence reveals that the land use degradation effects on the nitrous oxide release is complex and less significant in magnitude compared to methane and carbon dioxide.

In Fig. 4b, the magnitude, temporal evolution, and interannual variability of cumulative N_2O fluxes across land-use types show a relatively similar pattern during the rainy season, highlighting a weaker control by ecosystem management and soil-hydrological conditions. Nevertheless, there is a noticeable spatial heterogeneity at the Forest and Grassland sites, while the cumulative N_2O fluxes are less heterogeneous at the Cropland and Rice Fields. Compared to Cropland and Rice fields, Forest and grassland systems exhibit relatively low seasonal N_2O accumulation, consistent with their lower nitrogen inputs and more conservative nitrogen cycling. In forests, cumulative N_2O fluxes remain close to zero for much of the season, with modest net emissions emerging late in the rainy period, particularly in 2024 (0.02 kg C ha^{-1} $season^{-1}$).

The sensitivity of the cumulative N_2O fluxes to interannual differences in moisture regime or mineral nitrogen availability is shown as divergence between dashed (2023) and solid (2024) mean curves and their confidence envelopes. Higher cumulative emissions with increased spatial heterogeneity among chambers and episodic N_2O uptake early in the season is shown in the Grassland system. Especially in 2023, the wide confidence intervals underscore the importance of localized "hot spots" and "hot moments" in driving cumulative N_2O budgets even in low-input systems. However, a clearer monotonic increase through the rainy season with consistently higher cumulative N_2O emissions is observed at the Cropland and Rice Fields. Although there is a pronounced

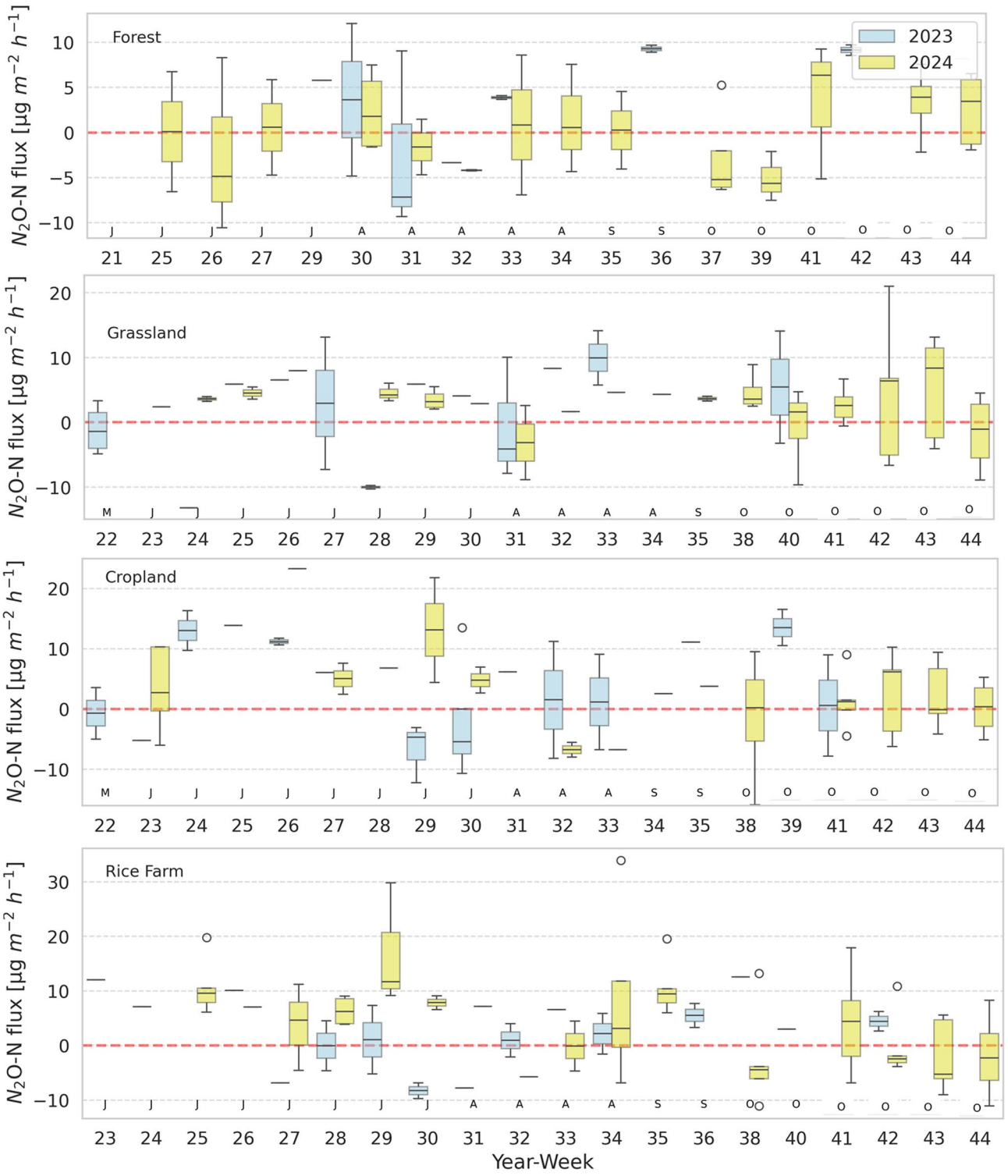

Fig. 5. Weekly boxplot time series of in situ N_2O flux for 2023 (light blue) and 2024 (yellow). Each boxplot is made of fluxes from 5 sub-trial points (chambers). From top to bottom are the forest reserve, grassland, cropland, and rice fields.

chamber-to-chamber variability, indicative of spatially heterogeneous microbial activity, Cropland exhibits a steady accumulation of N_2O in both years. Net N_2O uptake alongside strong emitters is observed exhibiting the coexisting differences between the chambers. This emphasizes the complexity of nitrogen transformations in flooded systems where denitrification can both produce and consume N_2O depending on redox conditions. The overall N_2O release observed across all land uses indicate that cumulative N_2O emissions are not solely driven by land-use type but are highly responsive to year-specific climatic conditions during the rainy season. These

findings reinforce the need for multi-chamber measurements to adequately capture ecosystem-scale emissions and avoid bias from localized extremes.

Soil moisture

The soil porosity depends on the bulk density, which is required in Eq. 2 to compute WFPS[25]. WFPS values are not calculated for the forest reserve because the bulk density was not measured. The highest annual mean soil moisture is observed at the rice fields (59.99% WFPS) while the lowest value occurred in the cropland (32.11% WFPS, Fig. 6). In response to increased dry spells in 2024, the annual mean soil moisture dropped by 32% (40.56% WFPS) in the rice fields. The grassland recorded a higher soil moisture (49.9% WFPS) within

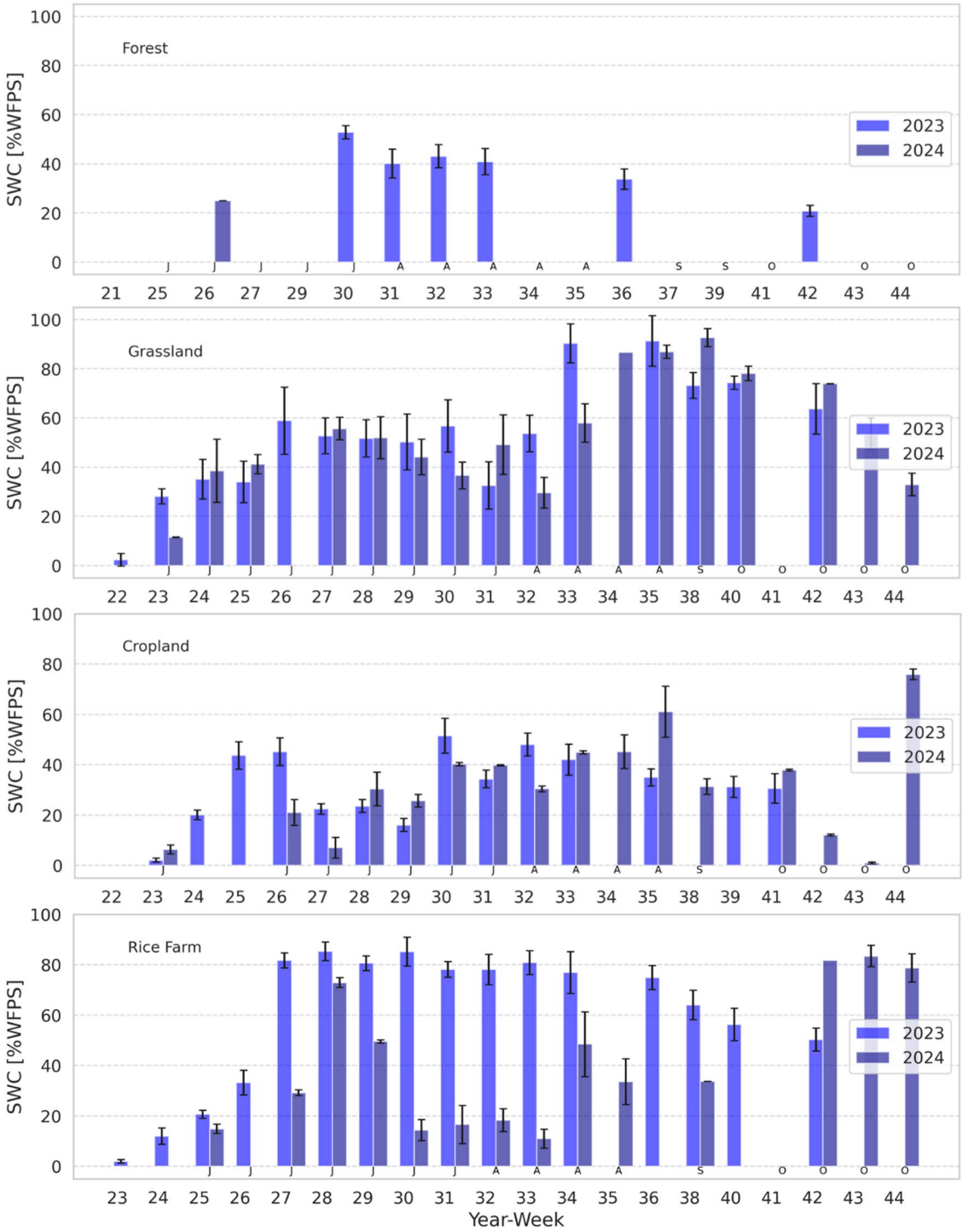

Fig. 6. Manually measured soil volumetric water content of the four sites for the two years. The soil moisture data were not fully collected noticeably at the forest site.

the same period. For the two years, the soil moisture peak occurred between August and September at the cropland (41.81/43.67% WFPS) and grassland (73.25/91.02% WFPS) which is associated with the higher rainfall period. The growing season started with relatively high soil moisture at the grassland site (39.01/27.88% WFPS) compared to the rice fields where lower values are recorded (16.94/15.69% WFPS) and this might explain the relatively strong emission observed in the grassland. Although the soil moisture annual mean at the cropland is 32.11% WFPS in 2023 and 28.33% WFPS in 2024 which are lower compared to the other sites, the emissions magnitude is even lower because of the soil disturbance by agricultural activities. In fact, similar practices are undertaken at the rice fields, yet higher emissions are observed. The rice field is in a lowland area where overland flow is delayed after intense rainfall which causes longer soil moisture period. This landscape characteristics is one of the reasons why soil moisture induced emissions is higher at the rice fields even with 56.7% lower rainfall (approximately 380 mm during the 2024 campaign).

Evaluation of environmental drivers of the fluxes

The Pearson correlation coefficients for soil water content and soil temperature are −0.85, −0.56, −0.59, and −0.38 respectively for the forest, grassland, cropland, and rice fields. The stepwise multi-linear regression indicates an overall performance of 0.58 ($p < 0.001$) at the grassland site (see Table 3). The soil temperature and water content explain 37% and 13% of the CH_4 flux, respectively. The two predictors have opposite effects on the flux, a unit increase in the soil water content increases the CH_4 flux by 0.41 µg C m^{-2} h^{-1} while decreases by −0.46 µg C m^{-2} h^{-1} for the soil temperature. The highest methane release occurred around 60% WFPS when the soil temperature ranges between 30 and 40 °C. Higher soil temperature (> 40 °C) with relatively low soil water content results in low CH_4 uptake or sink. Remarkably, high soil moisture (> 60%WFPS) with low temperature results in predominantly moderate methane release which was confirmed in past studies (Gütlein et al., 2018; Brümmer et al., 2009) at the grassland site. Moderate to low soil carbon content along with a positive soil moisture effect, are major factors controlling the annual average methane release over the two rainy seasons.

Although the temporal variability displays both CH_4 uptake and sink, the predictors explain 40% of the overall CH_4 flux ($p < 0.005$) and have similar effects as mentioned above at the cropland site. A unit increase of a predictor respectively increases CH_4 flux by 0.26 µg C m^{-2} h^{-1} for soil water content and decreases by −0.35 µg C m^{-2} h^{-1} for the temperature. The methane flux is explained by 0.21 ($p < 0.005$) and 0.37 ($p < 0.001$) respectively for soil water content and temperature. The predictors influence is less significant compared to the grassland which further confirms that emissions from perturbed soil disrupt the nitrification/denitrification process. Despite the moderate to low soil carbon content, the site displays methane sink for the two years (Table 2). Moderate soil temperature (30 to 40 °C) leads to higher CH_4 flux compared to lower soil temperature whatever the range of the soil water content (Fig. 7).

At the rice fields site, the highest influence of soil water content occurred as the variability is explained by 42% with a unit increase inducing a CH_4 flux of 0.96 µg C m^{-2} h^{-1}. The soil temperature effect is negative with a decrease of −0.85 µg C m^{-2} h^{-1} and explains 18% ($p < 0.005$) of the variability. The overall performance is moderate with a correlation coefficient of 0.5 ($p < 0.001$).

Moderate to low soil carbon content combined with the aforementioned factors resulted in annual average CH_4 release of 19.10 ± 4.7 and 22.5 ± 5.9 (µg C m^{-2} h^{-1}) for the two years. Above 30% WFPS, low soil temperatures lead to low uptake or release. Predominantly, in moderate temperature conditions, high soil water content leads to significantly high CH_4 release while lower soil moisture shows lower emission magnitude to sink.

	LCLU	Parameter	Coef.	Partial r^2	Adj. Partial r^2	p-value	r^2	Adj. r^2	p-value
CH_4	Forest	WFPS	–	–	–	–	–	–	–
		T_{soil}	–	–	–	–	–	–	–
	Grassland	WFPS	0.41	0.37	0.56	< 0.001	0.58	0.54	< 0.001
		T_{soil}	− 0.46	0.13					
	Cropland	WFPS	0.26	0.21	0.37	< 0.005	0.4	0.34	< 0.005
		T_{soil}	− 0.35	0.37		< 0.001			
	Rice fields	WFPS	0.96	0.42	0.48	< 0.001	0.5	0.47	< 0.001
		T_{soil}	− 0.85	0.18		< 0.005			
N_2O	Forest	WFPS	–	–	–	–	–	–	–
		T_{soil}	–	–	–	–			
	Grassland	WFPS	0.06	0.04	0.24	–	0.28	0.21	< 0.005
		T_{soil}	0.00	0.00		–			
	Cropland	WFPS	− 0.06	0.015	0.08	–	0.13	0.052	
		T_{soil}	0.13	0.07		–			
	Rice fields	WFPS	− 0.04	0.023	0.24	–	0.27	0.22	< 0.005
		T_{soil}	0.2	0.16		< 0.005			

Table 3. Stepwise multiple linear regression between in situ fluxes (CH_4 and N_2O), soil water content (% WFPS), and soil temperature (°C) for each land use.

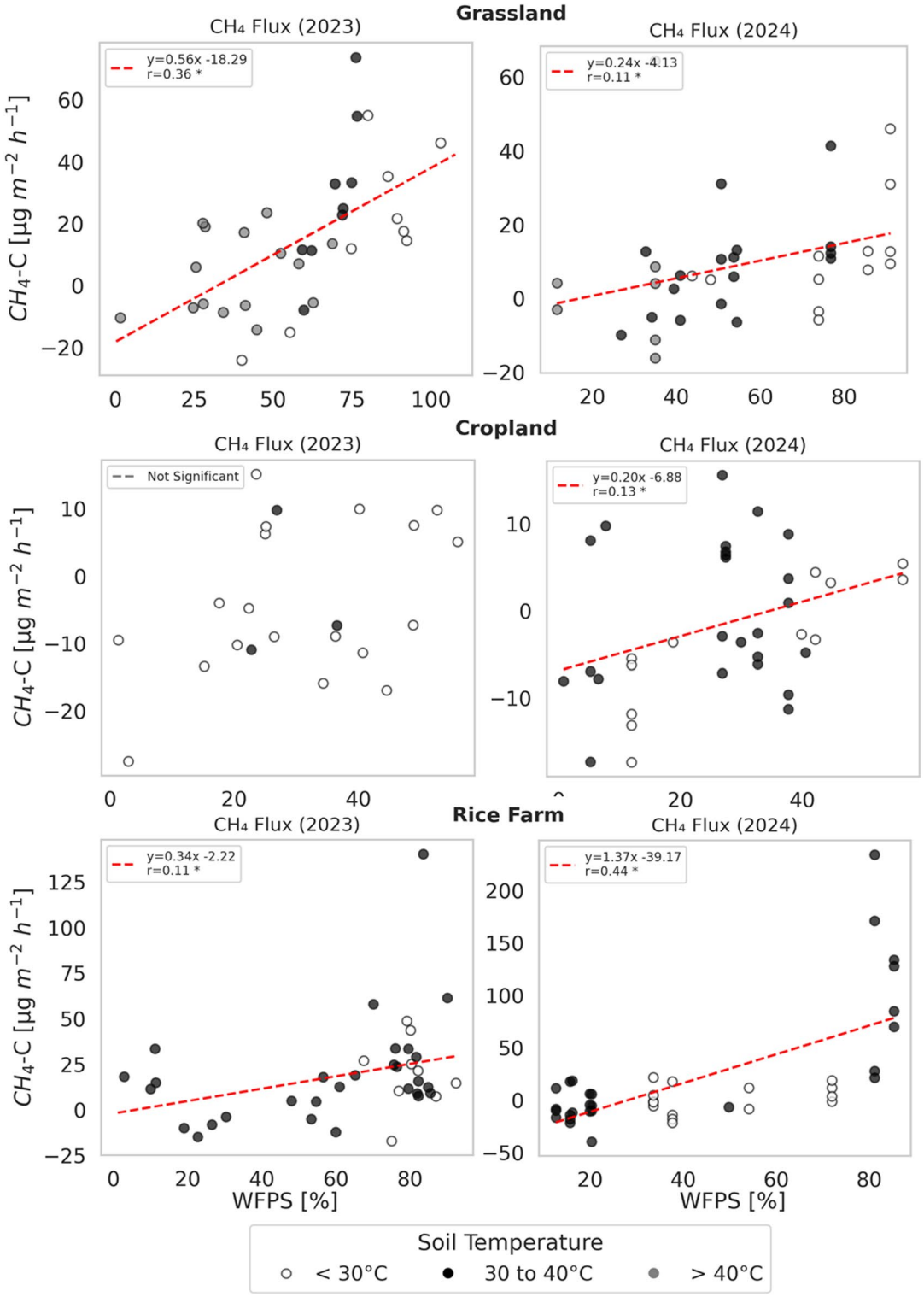

Fig. 7. CH_4 response to soil moisture change (% WFPS) and soil temperature classified into three categories for 2023 and 2025. Linear regression is displayed in red if the relationship is significant with corresponding r value.

The performance of the stepwise multi-linear regression multi-linear is relatively low (0.13–0.28) for N_2O flux, whatever the land use. The soil water content and temperature have opposite effects on N_2O emissions. A unit increase of each predictor leads to −0.06 and −0.04 µg N m^{-2} h^{-1} decrease in N_2O flux, respectively for the cropland and rice fields. The soil temperature increases N_2O flux respectively by 0.13 and 0.2 µg N m^{-2} h^{-1}(Fig. 8). Despite the low soil nitrogen content with less significant soil moisture and temperature effects on

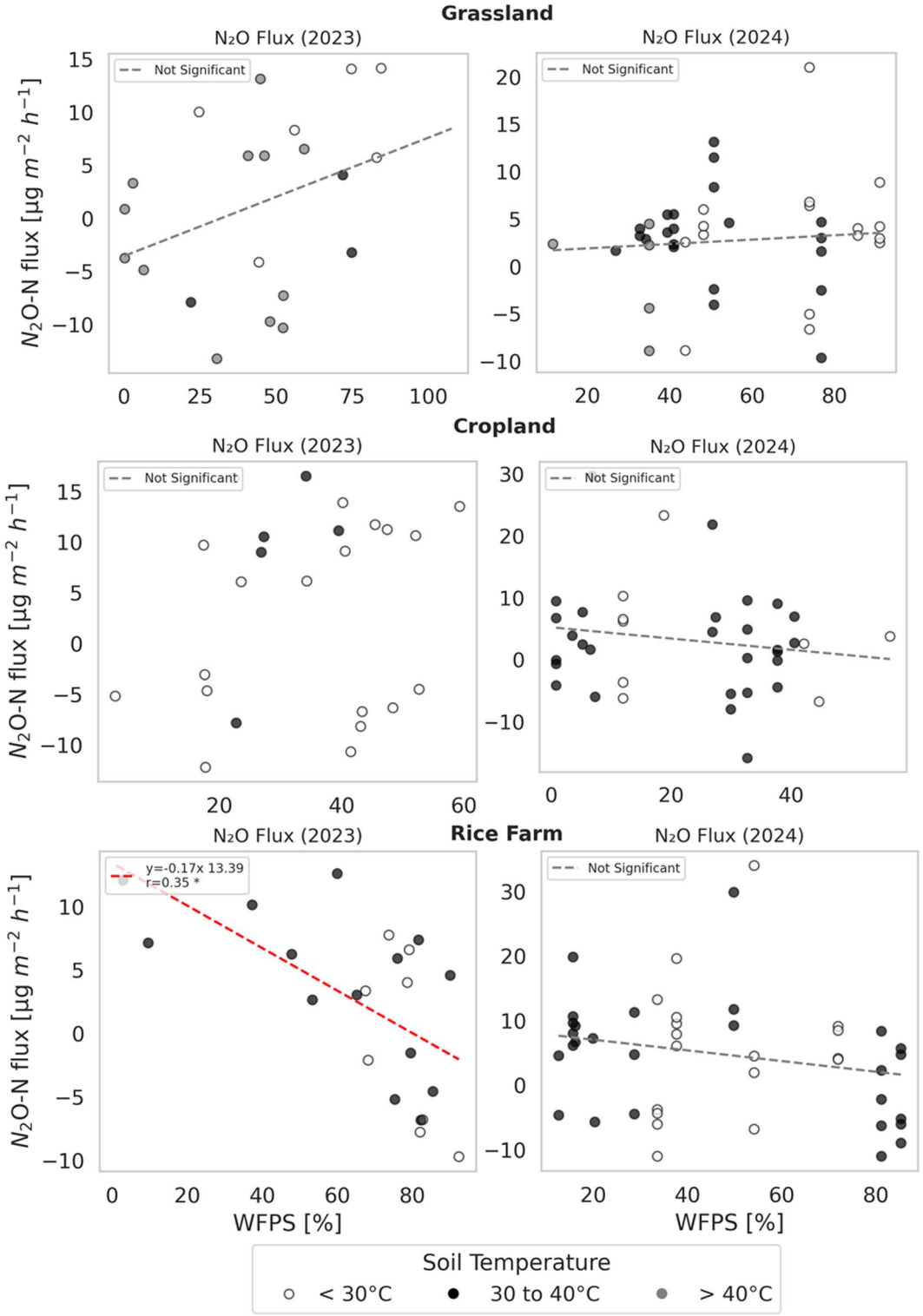

Fig. 8. N_2O response to soil moisture change (% WFPS) and soil temperature classified into three categories for 2023 and 2025. Linear regression is displayed in red if the relationship is significant with corresponding r value.

N_2O, the investigated sites altogether are N_2O sources (Table 2) with no significant difference in mean N_2O flux. There is no significant linear relationship between soil water content and N_2O emissions except at the rice fields site where higher soil water content and moderate soil temperature led to N_2O sink for the two years. Similar conditions associated with lower soil water content (< 40% WFPS) result in N_2O release. Below 30 °C, the N_2O flux is mitigated as both uptake and sink occur. However, the highest N_2O flux occurs between 40

and 60% WFPS at the rice fields site. Moderate soil temperature with low soil moisture (< 30% WFPS) leads predominantly to N_2O release at the cropland site.

Discussions

This study provides site-specific assessment of soil greenhouse gas emissions across two consecutive rainy seasons (2023–2024) in four contrasting land-use types within the West African Sudanian savanna. Importantly, it includes, for the first time, measurements from a rainfed paddy rice cultivation system, widely recognized as a major source of methane emissions (Guug et al. 2025), alongside savanna forest, cropland, and grassland ecosystems. Our results demonstrate that soil at the grassland site was a net source of methane whereas the managed cropland site behaves as a sink. Monthly variation of the emissions reveals that both uptake and release occur depending on soil water content in response to rainfall events. In a typical cleared savanna, it has been demonstrated that the soil behaves as a net methane source[56–60]. which aligns with our observed CH_4 release at the grassland site (14.44 ± 9.6 and 10.13 ± 3.5 μg C m^{-2} h^{-1}). Remarkably, the unperturbed soil of the Sudanian savanna displays significant methane release while the cultivated cropland indicates a net methane sink (−1.78 ± 5.5 and − 2.05 ± 3.8 μg C m^{-2} h^{-1}), similar to results reported by Brümmer et al., (2008 and 2009)[24,61] in south Sudanian savanna of Burkina Faso. Furthermore, Castaldi et al. (2004)[62] demonstrated similar evidence in an herbaceous savanna (7.2 μg C m^{-2} h^{-1}) and cultivated pasture (−1.5 μg C m^{-2} h^{-1}) of Orinoco (Venezuela) unlike Sanhueza and Donoso (2006)[63] who reported the opposite in a tropical savanna respectively − 12.6 and 16.2 μg C m^{-2} h^{-1}. In addition, the woodland savanna methane sink (−2.5 μg C m^{-2} h^{-1}) reported by Castaldi et al. (2004)[62] also corroborates our observation at the forest reserve (−0.52 ± 5.5 and − 11.48 ± 3.6 μg C m^{-2} h^{-1}). An average methane sink rate of −40 to −12 μg C m^{-2} h^{-1} was reported in managed and natural savanna systems[64–66] which confirms both the observation at the cropland and forest reserve. Castaldi et al. (2006)[67] assessed the uncertainties related to the soil-atmosphere methane exchange in the tropical savanna confirming the relatively wide range. Our results revealed that significant methane release occurred at the rainfed rice fields (19.10 ± 4.7 and 22.5 ± 5.9 μg C m^{-2} h^{-1}) compared to the other sites for the two years. However, the soil CH_4 flux is significantly less than the reported values (0.2 to 99 mg C m^{-2} h^{-1}) for flooded rice fields[55,68,69].

Moreover, this study builds upon and extends the work of Brümmer et al. (2008) by re-examining CH_4 and N_2O emissions across four contrasting land-use types in the Sudanian savanna of West Africa. Across four sites the annual mean of N_2O emissions varies between 0.011 ± 0.11 and 0.16 ± 0.31 kg N ha^{-1} $season^{-1}$ which aligns with the range reported for a tropical savanna (0.06 to 1.46 kg N ha^{-1} yr^{-1}) by Dalal and Allen (2008)[70,71], for Australian savannas (0.06–1.08 kg N ha^{-1} yr^{-1}) by Werner et al. (2014)[25], and in near-natural and agricultural land of Burkina Faso (0.18 and 0.7 kg N ha^{-1} yr^{-1}) by Brümmer et al. (2008)[24]. Notwithstanding, the ongoing debate on the controlling factors, it is reported that either low rainfall or low nitrogen content or the combined effect narrows the N_2O release or sink[25,30,63,72–74]. In high rainfall conditions, the suggestion that low soil nitrogen content limits N_2O emissions[75] corroborates our findings. The nitrogen content at the grassland, cropland, and rice fields sites is low limiting the emissions.

Except for the forest reserve, a strong signal of N_2O emissions is observed during the rainfall onset in June (see Table 2). This finding is consistent with previous studies showing that, in tropical ecosystems, the first rainfall events at the end of the dry season trigger pronounced N_2O emission pulses due to the accumulation of ammonium (NH_4^+) and nitrate (NO_3^-) in soils during prolonged dry periods (e.g., Calvo-Rodriguez et al. (2020)[51,67,76] in Brümmer et al. (2008)[24]. Similar CH_4 flux dependence on soil moisture was demonstrated in South Sudanian savanna by Brümmer et al., (2009). This response to a sudden increase in soil moisture due to intense microbial activity after relatively long period of water-stress[77] is also reported in the savanna woodlands of Zimbabwe[78]. The soil nitrogen content at the grassland, cropland, and rice fields sites is relatively low (Fig. S2). Therefore, the nitrification and denitrification in the soils are limited by poor substrate availability which narrows the factors evaluated in this study to mainly the soil moisture and temperature.

Strong contrasts in both magnitude and temporal dynamics are shown in the cumulative fluxes of CH_4 across the investigated land use types, highlighting the combined roles of hydrological regime, land management, and soil biogeochemical controls. Sustained anaerobic conditions favor methanogenesis with the strongest cumulative CH_4 emissions particularly during mid- to late-season flooding at the Rice fields. In contrast, well-aerated soils associated with active methanotrophic consumption in the case of the Forest showed predominantly negative CH_4 fluxes, acting as net methane sinks throughout most of the season. With site-level heterogeneity indicating localized controls, the Cropland displayed intermediate and more variable CH_4 responses related to the spatial variability of soil moisture, compaction, and organic substrate availability. However, a nearly homogeneous release pattern in the cumulative CH_4 fluxes is clearly displayed at the Grassland site.

Cumulative N_2O fluxes exhibited smaller absolute magnitudes than CH_4 but showed noticeable similarity between the temporal pattern and magnitude across the land-use types. Cropland and Rice fields generally accumulated higher N_2O emissions than Forests and Grasslands which is consistent with enhanced nitrogen availability and episodic denitrification under fluctuating redox conditions. Remarkably, the temporal evolution of N_2O differed from CH_4, with the land use types exhibiting early-season accumulation followed by stabilization or reversal, suggesting shifts between nitrification- and denitrification-dominated pathways as soil moisture and temperature evolved. The spatial heterogeneity of GHG production within land use types is emphasized by the chamber-level variability and confidence intervals. The contrasting patterns between 2023 and 2024 indicate a strong sensitivity of both gases to interannual climatic variability. Altogether, these results demonstrate that land-use type governs the dominant greenhouse gas pathway during the rainy season, with CH_4 dominating climate forcing in flooded systems and N_2O contributing disproportionately in managed upland soils when expressed in CO_2-equivalent terms (Fig. S3a-b).

The nitrogen isotopic ratio $\delta^{15}N$ of the soil profiles collected at the grassland, cropland, and rice fields indicates that they receive enriched animal manure with losses resulting from nitrification and denitrification

processes leading to further enrichments of the soil $\delta^{15}N$ (Fig. S2). The values of the $\delta^{15}N$ ratio vary between 3.0 and 5.6‰ with an average of 4.1 ± 0.5‰ at the cropland site, 1.9 and 5.2‰ with an average of 3.8 ± 0.4‰ at the grassland site, and 2.0 and 6.0‰ with an average of 3.9 ± 0.4‰ at the rice fields (Fig. S2). This finding is also consistent with previous studies, including the investigations of Gerschlauer et al. (2019)[54], which reported similar soil responses across the Mount Kilimanjaro elevation range (0–8‰), thereby corroborating our results. Similar evidence is reported recently in a heterogeneous landscape of the Schwingbach catchment[79]. Though the profiles display similar nitrogen $\delta^{15}N$ ratios, the nitrogen content is relatively low for the three sites (Fig. S2). The average nitrogen content values are respectively 0.04 ± 0.01%, 0.04 ± 0.01%, and 0.05 ± 0.01% for the grassland, cropland, and rice fields, respectively. This low level of nitrogen substrate availability is a major factor that justifies the consequent limited N_2O emissions.

Conclusions and policy implications

At the regional scale, this study provides important insights for climate assessment, land management, and policy development in West Africa, a region where observational data on land-atmosphere greenhouse gas (GHG) exchanges remain scarce. By quantifying soil CH_4 and N_2O fluxes across four dominant land-use types in the Sudanian savanna over two consecutive rainy seasons (2023–2024), this work extends earlier regional assessments (e.g., Brümmer et al., 2008, Yaro et al., 2024)[21,24,80–82]. Notably, it incorporates, for the first time, measurements from a rainfed paddy rice system, which is widely recognized as a significant source of methane emissions, alongside savanna forests, croplands, and grassland ecosystems. The results reveal that methane dynamics are strongly shaped by land use. Rainfed paddy rice systems emerged as the largest CH_4 sources, highlighting the key role of soil water saturation in creating anaerobic conditions favorable to methanogenesis[2]. In contrast, the forest reserve primarily functioned as a methane sink, while grassland ecosystems acted as net sources with pronounced temporal variability driven by fluctuations in soil moisture and temperature. Cropland soils exhibited comparatively low methane fluxes and frequently behaved as weak sinks, suggesting that cultivation practices can suppress CH_4 emissions relative to unmanaged grasslands. Across all land-use types, soil water content was identified as the dominant control on methane fluxes, particularly during rainfall onset, whereas soil temperature exerted a secondary but opposing influence, most notably in rice systems. In contrast, nitrous oxide emissions remained consistently low and showed no significant differences among land-use types or between years. This pattern indicates that limited soil nitrogen availability constrains N_2O production in the Sudanian savanna, reducing the sensitivity of emissions to soil moisture and temperature relative to nitrogen-rich ecosystems. Under current management conditions, these findings suggest that though N_2O magnitude in kg N ha^{-1} $season^{-1}$ might be less than the CH_4 in kg C ha^{-1} $season^{-1}$, it contributes significantly more to the regional GHG balance than methane in terms of the global warming potential in CO_2-equivalent. Following the IPCC AR6 global warming potentials, we show that non-CO_2 greenhouse gas emissions from agricultural land uses exert a disproportionate influence on seasonal CO_2-equivalent budgets compared to natural ecosystems. Our findings emphasize that effective climate mitigation in tropical landscapes requires integrated management approaches targeting both CH_4 production under anaerobic conditions and N_2O emissions driven by nitrogen cycling. From a policy and land-management perspective, these results underscore the importance of land-use-specific mitigation strategies rather than uniform approaches. Rice cultivation represents a clear methane emission hotspot, indicating substantial mitigation potential through improved water management practices such as intermittent flooding or drainage. Conversely, conserving forest cover can enhance methane uptake, reinforcing the climate mitigation value of forest protection. Grassland management strategies that minimize prolonged soil saturation may further help reduce episodic methane emissions.

Limitations

Capturing fully the heterogeneity of soils, management practices, and microclimatic conditions across the broader Sudanian savanna region remain a challenge despite the spatial scope and temporal frequency of the measurements. Only the rainy seasons were covered for two years and temporal resolution was restricted to weekly excluding dry-season fluxes and short-lived emission pulses following extreme rainfall that could influence annual greenhouse gas budgets. Absence of detailed measurements of soil nitrogen transformations and microbial processes constrains the mechanistic interpretation of N_2O dynamics. This limits the ability to generalize controls beyond the observed environmental drivers.

Data availability

The datasets generated and/or analysed during the current study are available from the corresponding author upon reasonable request.

Received: 1 June 2025; Accepted: 10 January 2026
Published online: 28 February 2026

References

1. Canadell, J. G. et al. Global carbon and other biogeochemical cycles and feedbacks. In *Climate Change 2021: The Physical Science Basis. Contribution of Working Group I to the Sixth Assessment Report of the Intergovernmental Panel on Climate Change* (eds Masson-Delmotte, V. et al.) 673–816 https://refhub.elsevier.com/S0048-9697(22)04639-3/-rf202207230300244030 (Cambridge University Press, 2021).
2. Guug, S. et al. Methane emissions from rice cultivation in West Africa and compensation options from nature reserve forests. *Environ. Res. Lett.* **20** (4), 044050. https://doi.org/10.1088/1748-9326/adc28c (2025).
3. Tharammal, T., Bala, G., Devaraju, N. & Nemani, R. A review of the major drivers of the terrestrial carbon uptake: Model-based assessments, consensus, and uncertainties. *Environ. Res. Lett.* **14** (9), 093005. https://doi.org/10.1088/1748-9326/ab3012 (2019).

4. NOAA. National Oceanic and Atmospheric Administration. https://refhub.elsevier.com/S0048-9697(22)04639-3/-rf20220723025 5438636 (2020).
5. Heilig, G. K. The greenhouse gas methane (CH4): sources and sinks, the impact of population growth, possible interventions. *Popul. Environ.* **16** (2), 109–137. https://doi.org/10.1007/bf02208779 (1994).
6. Xu, X. et al. Reviews and syntheses: four decades of modeling methane cycling in terrestrial ecosystems. *Biogeosciences* **13**, 3735–3755. https://doi.org/10.5194/bg-13-3735-2016 (2016).
7. Dutaur, L. & Verchot, L. V. A global inventory of the soil CH4 sink. *Glob. Biogeochem. Cycles*. https://doi.org/10.1029/2006GB002734 (2007).
8. IPCC. Summary for policymakers. In *Climate Change and Land: An IPCC Special Report on Climate Change, Desertification, Land Degradation, Sustainable Land Management, Food Security, and Greenhouse Gas Fluxes in Terrestrial Ecosystems* (eds Shukla, P.R. et al.) In press. (2019).
9. Butterbach-Bahl, K., Baggs, E. M., Dannenmann, M., Kiese, R. & Zechmeister-Boltenstern, S. Nitrous oxide emissions from soils: how well do we understand the processes and their controls?. *Philos. Trans. R. Soc. B.* **368**, 20130122. https://doi.org/10.1098/rstb.2013.0122 (2013).
10. Schaufler, G. et al. Greenhouse gas emissions from European soils under different land use: effects of soil moisture and temperature. *Eur. J. Soil. Sci.* **61**, 683–696. https://doi.org/10.1111/j.1365-2389.2010.01277.x (2010).
11. Ma, R. et al. Data-driven estimates of fertilizer-induced soil NH3, NO, and N2O emissions from croplands in China and their climate change impacts. *Glob Chang. Biol.* **28**, 1008–1022. https://doi.org/10.1111/gcb.15975 (2022).
12. Schlesinger, W. H. An estimate of the global sink for nitrous oxide in soils. *Glob Chang. Biol.* **19**, 2929–2931. https://doi.org/10.1111/gcb.12239 (2013).
13. Schwenke, G. D. et al. Soil N2O emissions under N2-fixing legumes and N-fertilised canola: a reappraisal of emissions factor calculations. *Agric. Ecosyst. Environ.* **202**, 232–242. https://doi.org/10.1016/j.agee.2015.01.017 (2015).
14. Eichner, M. L. Nitrous oxide emissions from fertilized soils: summary of available data. *J. Environ. Qual.* **19**, 272–280 (1990).
15. Officer, S. J. et al. Response of soil nitrous oxide flux to nitrogen fertiliser application and legume rotation in a semi-arid climate, identified by smoothing spline models. *Soil. Res.* **53**, 227–241 (2015).
16. Nicolardot, B., Guinet, M., Voisin, A-S. & Hénault, C. N_2O emission pattern in a legume-based agroecosystem. *Adv. Environ. Eng. Res.* https://doi.org/10.21926/aeer.2302029 (2023).
17. Jensen, E. S., Peoples, M. B., Boddey, R. M., Gresshoff, P. M. & Hauggaard-Nielsen, H. Legumes for mitigation of climate change and the provision of feedstock for biofuels and biorefineries. A review. *Agron. Sustain. Dev.* **32**, 329–364 (2012).
18. Senbayram, M. et al. Legume-based mixed intercropping systems may lower agricultural born N2O emissions. *Energy Sustain. Soc.* **6**, 2 (2015).
19. Maier, R., Hörtnagl, L. & Buchmann, N. Greenhouse gas fluxes (CO2, N2O and CH4) of pea and maize during two cropping seasons: Drivers, budgets, and emission factors for nitrous oxide. *Sci. Total Environ.* **849**, 157541. https://doi.org/10.1016/j.scitotenv.2022.157541 (2022).
20. Sy, S. et al. Land-surface characteristics and climate in West Africa: models' biases and impacts of historical anthropogenically-induced deforestation. *Sustainability.* **9**(10), 1917. https://doi.org/10.3390/su9101917 (2017).
21. Sy, S. & Quesada, B. Anthropogenic land cover change impact on climate extremes during the 21st century. *Environ. Res. Lett.* **15** (3), 034002. https://doi.org/10.1088/1748-9326/ab702c (2020).
22. Merbold, L. et al. Greenhouse gas budget (CO2, CH4 and N2O) of intensively managed grassland following restoration. *Glob Chang. Biol.* **20**, 1913–1928. https://doi.org/10.1111/gcb.12518 (2014).
23. Merbold, L. et al. Greenhouse gas budget (CO_2, CH_4 and N_2 O) of intensively managed grassland following restoration. *Glob. Change Biol.* **20** (6), 1913–1928. https://doi.org/10.1111/gcb.12518 (2014).
24. Brümmer, C. et al. Soil-atmosphere exchange of N2O and NO in near-natural savanna and agricultural land in Burkina Faso (W. Africa). *Ecosystems*. **11**(4), 582–600. https://doi.org/10.1007/s10021-008-9144-1 (2009).
25. Werner, C. et al. N_2O, NO, N_2, and CO_2 emissions from tropical savanna and grassland of northern Australia: An incubation experiment with intact soil cores. *Biogeosciences* **11** (21), 6047–6065. https://doi.org/10.5194/bg-11-6047-2014 (2014).
26. Conrad, R. Soil microorganisms as controllers of atmospheric trace gases (H2, CO, CH4, OCS, N2O, and NO). *Microbiol. Rev.* **60**, 609–640 (1996).
27. Baggs, E. M. Review of stable isotope techniques for N2O source partitioning in soils: recent progress, remaining challenges and future considerations. *Rapid Commun. Mass. Sp.* **22**, 1664–1672 (2008).
28. Grover, S. P. P. et al. Land use change and the impact on greenhouse gas exchange in North Australian savanna soils. *Biogeosciences* **9**, 423–437. https://doi.org/10.5194/bg-9-423-2012 (2012).
29. Werner, C., Kiese, R. & Butterbach-Bahl, K. Soil–atmosphere exchange of N2O, CH4, and CO2 and controlling environmental factors for tropical rain forest sites in western Kenya. *J. Geophys. Res.* **112**, D03308. https://doi.org/10.1029/2006JD007388 (2007).
30. Andersson, M., Kjøller, A. & Struwe, S. Soil emissions of nitrous oxide in fire-prone African savannas. *J. Geophys. Res. Atmos.* **108**, 4630. https://doi.org/10.1029/2002JD003345 (2003).
31. Pachauri, R. K. et al. Climate change 2014: synthesis report. Contribution of Working Groups I, II and III to the fifth assessment report of the Intergovernmental Panel on Climate Change (IPCC, 2014).
32. Tian, H. et al. A comprehensive quantification of global nitrous oxide sources and sinks. *Nature* **586**, 248–256. https://doi.org/10.1038/s41586-020-2780-0 (2020).
33. Grossi, G., Goglio, P., Vitali, A. & Williams, A. G. Livestock and climate change: impact of livestock on climate and mitigation strategies. *Anim. Front.* **9**, 69–76 (2018).
34. Flechard, C. et al. Effects of climate and management intensity on nitrous oxide emissions in grassland systems across Europe. *Agric. Ecosyst. Environ.* **121**, 135–152. (2007).
35. Murphy, R. M. et al. Nitrous oxide emission factors from an intensively grazed temperate grassland: A comparison of cumulative emissions determined by eddy covariance and static chamber methods. *Agric. Ecosyst. Environ.* **324**, 107725. https://doi.org/10.1016/j.agee.2021.107725 (2022).
36. Carpinelli, S., Da Fonseca, A. F., Weirich Neto, P. H., Dias, S. H. B. & Pontes, L. D. S. Spatial and temporal distribution of cattle dung and nutrient cycling in integrated crop–livestock systems. *Agronomy.* **10**, 672 (2020).
37. Maire, J. et al. Identifying urine patches on intensively managed grassland using aerial imagery captured from remotely piloted aircraft systems. *Front. Sustain. Food Syst.* **2**, 2 (2018).
38. Hyde, B. et al. The interactive effects of fertiliser nitrogen with dung and urine on nitrous oxide emissions in grassland. *Ir. J. Agric. Food Res.* **55**, 1–9 (2016).
39. Jarvis, S., Scholefield, D. & Pain, B. Nitrogen cycling in grazing systems. In *Nitrogen Fertilization in the Environment* (ed Bacon, P. E.) 381–419. https://refhub.elsevier.com/S0167-8809(21)00429-1/sbref32 (Marcel Dekker, 1995).
40. O'connell, K., Humphreys, J. & Watson, C. J. Quantification of nitrogen sources for grassland. *Winter Sci. Meet Fertil. Assoc. Irel.* 15–28 https://refhub.elsevier.com/S0167-8809(21)00429-1/sbref51 (2004).
41. Bliefernicht, J. et al. The WASCAL hydro-meteorological observatory in the Sudan savanna of Burkina Faso and Ghana. *Vadose Zone J.* https://doi.org/10.2136/vzj2018.03.0065 (2018).
42. Berger, S. et al. The impact of rain events on CO2 emissions from contrasting land use systems in semi-arid West African savannas. *Sci. Total Environ.* **647**, 1478–1489. https://doi.org/10.1016/j.scitotenv.2018.07.397 (2019).

43. Quansah, E. et al. Carbon dioxide fluxes from contrasting ecosystems in the Sudanian savanna in West Africa. *Carbon Balance Manag.* https://doi.org/10.1186/s13021-014-0011-4 (2015).
44. Nadolski, L. et al. Exploring and closing the energy balance of eddy covariance measurements along a land use gradient in the West African Sudanian savanna. *Front. Water*. **6**, 1393884 (2024).
45. Sultan, B. & Janicot, S. The West African monsoon dynamics, part II: the pre-onset and the onset of the summer monsoon. *J. Clim.* **16**, 3407–3427 (2003).
46. Nicholson, S. E. The West African Sahel: a review of recent studies on the rainfall regime and its interannual variability. *ISRN Meteorol.* **2013**, 1–32. https://doi.org/10.1155/2013/453521 (2013).
47. Bliefernicht, J. et al. Towards a historical precipitation database for West Africa: Overview, quality control and harmonization. *Int. J. Climatol.* **42** (7), 4001–4023. https://doi.org/10.1002/joc.7467 (2022).
48. De Klein, C. & Harvey, M. *Nitrous oxide Chamber Methodology and Guidelines*. https://refhub.elsevier.com/S0167-8809(21)00429-1/sbref18 (Ministry for Primary Industry, 2015).
49. Weller, S. et al. Diurnal patterns of methane emissions from paddy rice fields in the Philippines. *J. Plant Nutr. Soil Sci.* **178** (5), 755–767. https://doi.org/10.1002/jpln.201500092 (2015).
50. Charteris, A. F. et al. Global Research Alliance N2O chamber methodology guidelines: recommendations for deployment and accounting for sources of variability. *J. Environ. Qual.* **49**, 1092–1109 (2020).
51. Calvo-Rodriguez, S., Kiese, R. & Sánchez-Azofeifa, G. A. Seasonality and budgets of soil greenhouse gas emissions from a tropical dry forest successional gradient in Costa Rica. *J. Geophys. Res. Biogeosci.* https://doi.org/10.1029/2020jg005647 (2020).
52. Parkin, T. B., Venterea, R. T. & Hargreaves, S. K. Calculating the detection limits of chamber-based soil greenhouse gas flux measurements. *J. Environ. Qual.* **41**, 705–715. https://doi.org/10.2134/jeq2011.0394 (2012).
53. Bläsing, M. & Amelung, W. Plastics in soil: analytical methods and possible sources. *Sci. Total Environ.* **612**, 422–435. https://doi.org/10.1016/j.scitotenv.2017.08.086 (2018).
54. Gerschlauer, F. et al. Stable carbon and nitrogen isotopic composition of leaves, litter, and soils of various ecosystems along an elevational and land-use gradient at Mount Kilimanjaro. *Tanzan. Biogeosciences*. **16** (2), 409–424. https://doi.org/10.5194/bg-16-409-2019 (2019).
55. IPCC. Guidelines for National Greenhouse Gas Inventories. Reference Manual. (1996).
56. Zepp, R. G. et al. Effects of moisture and burning on soil-atmosphere exchange of trace carbon gases in a Southern African savanna. *J. Geophys. Res.* **101** (699–23,706). https://doi.org/10.1029/95JD01371 (1996).
57. Sanhueza, E., Ca´rdenas, L., Doloso, L. & Santana, M. Effect of plowing on CO_2, CO, CH_4, N_2O, and NO fluxes from tropical Savannah soils. *J. Geophys. Res.* **99** (429–16,434). https://doi.org/10.1029/94JD00265 (1994).
58. Poth, M., Anderson, I. C., Miranda, H. S., Miranda, A. C. & Riggan, P. G. The magnitude and persistence of soil NO, N2O, CH4 and CO2 fluxes from burned tropical savanna in Brazil, global biogeochem. *Cycles* **9**, 503–513. https://doi.org/10.1029/95GB02086 (1995).
59. Scharffe, D., Hao, W. M., Donoso, L., Crutzen, P. J. & Sanhueza, E. Soil fluxes and atmospheric concentrations of CO and CH4 in the Northern part of the Guayana shield. *Venezuela J. Geophys. Res.* **95** (475 22,480). https://doi.org/10.1029/JD095iD13p22475 (1990).
60. Hao, W. M., Scharffe, D., Crutzen, P. J. & Sanhueza, E. Production of N2O, CH4, and CO2 from soils in the tropical savanna during the dry season. *J. Atmos. Chem.* **7**, 93–105. https://doi.org/10.1007/BF00048256 (1988).
61. Brümmer, C., Papen, H., Wassmann, R. & Brüggemann, N. Fluxes of CH_4 and CO_2 from soil and termite mounds in South Sudanian savanna of Burkina Faso (West Africa). *Glob. Biogeochem. Cycles*. **23**(1), 2008GB003237. https://doi.org/10.1029/2008GB003237 (2009).
62. Castaldi, S. et al. Nitrous oxide and methane fluxes from soils of the orinoco savanna under different land uses. *Global Change Biol.* **10**, 1947–1960. https://doi.org/10.1111/j.1365-2486.2004.00871.x (2004).
63. Sanhueza, E. & Donoso, L. Methane emission from tropical savanna *Trachypogon* sp. grasses. *Atmos. Chem. Phys.* **6**, 5315–5319 (2006).
64. Tathy, J. P. et al. CH4 emission from flooded forest in central Africa. *J. Geophys. Res.* **97**, 6159–6168 (1992).
65. Keller, M., Veldkamp, E., Weitz, A. M. & Reiners, W. A. Effect of pasture age on soil trace-gas emissions from a deforested area of Costa Rica. *Nature* **365**, 244–246. https://doi.org/10.1038/365244a0 (1993).
66. MacDonald, J. A., Eggleton, P., Bignell, D. E., Forzi, F. & Fowler, D. Methane emission by termites and oxidation by soils, across a forest disturbance gradient in the Mbalmayo forest reserve, Cameroon. *Global Change Biol.* **4**, 409–418. https://doi.org/10.1046/j.13652486.1998.00163.x (1998).
67. Castaldi, S., Ermice, A. & Strumia, S. Fluxes of N_2O and CH_4 from soils of savannas and seasonally-dry ecosystems. *J. Biogeogr.* **33**, 401–415. https://doi.org/10.1111/j.1365-2699.2005.01447.x (2006).
68. Nikolaisen, M. et al. Methane emissions from rice paddies globally: A quantitative statistical review of controlling variables and modelling of emission factors. *J. Clean. Prod.* **409**, 137245. https://doi.org/10.1016/j.jclepro.2023.137245 (2023).
69. Lee, J. H., Lee, J. Y., Kang, Y. G., Kim, J. H. & Oh, T. K. Evaluating methane emissions from rice paddies: A study on the cultivar and transplanting date. *Sci. Total Environ.* **902**, 166174. https://doi.org/10.1016/j.scitotenv.2023.166174 (2023).
70. Dalal, R. C. & Allen, D. E. Turner review no. 18, greenhouse gas fluxes from natural ecosystems. *Aust. J. Bot.* **56**, 369–407 (2008).
71. Dannenmann, M., Gasche, R., Ledebuhr, A. & Papen, H. Effects of forest management on soil N cycling in beech forests stocking on calcareous soils. *Plant Soil* **287**, 279–300 (2006).
72. Donoso, L., Santana, R. & Sanhueza, E. Seasonal-variation of N2O fluxes at a tropical savanna site – soil consumption of N2O during the dry season. *Geophys. Res. Lett.* **20**, 1379–1382 (1993).
73. Livesley, S. J. et al. Seasonal variation and fire effects on CH4, N2O and CO2 exchange in savanna soils of Northern Australia. *Agric. For. Meteorol.* **151**, 1440–1452 (2011).
74. Sanhueza, E., Hao, W. M., Scharffe, D. H., Donoso, L. & Crutzen, P. J. N2O and NO emissions from soils of the northern part of the Guayana shield, Venezuela. *J. Geophys. Res.* **95**, 22481–22488 (1990).
75. Rosenkranz, P. et al. N2O, NO and CH4 exchange, and microbial N turnover over a Mediterranean pine forest soil. *Biogeosciences* **3**(121–133), 2006. https://doi.org/10.5194/bg-3-121-2006 (2006).
76. Scholes, M. C., Martin, R., Scholes, R. J., Parsons, D. & Winstead, E. NO and N2O emissions from savanna soils following the first simulated rains of the season. *Nutr. Cycl. Agroecosys.* **48**, 11522 (1997).
77. Ludwig, J., Meixner, F. X., Vogel, B. & Forstner, J. Soil–air exchange of nitric oxide: an overview of processes, environmental factors, and modeling studies. *Biogeochemistry* **52**, 225–257 (2001).
78. Rees, R. M., Wuta, M., Furley, P. A. & Li, C. Nitrous oxide fluxes from savanna (miombo) woodlands in Zimbabwe. *J. Biogeogr.* **33**, 424–437 (2006).
79. Wangari, E. et al. Spatial-temporal patterns of foliar and bulk soil 15 N isotopic signatures across a heterogeneous landscape: linkages to soil N status, nitrate leaching, and N2O fluxes. *Soil Biol. Biochem.* **199**, 109609. https://doi.org/10.1016/j.soilbio.2024.109609 (2024).
80. Yaro, V. S. O. et al. Greenhouse gas emission from prescribed fires is influenced by vegetation types in West African savannas. *Sci. Rep.* **14** (1), 23754. https://doi.org/10.1038/s41598-024-73753-6 (2024).
81. Yahaya Seydou, A. N. et al. Biophysical effects of land cover changes in West africa: A systematic review. *Environ. Res. Lett.* https://doi.org/10.1088/1748-9326/addbf4 (2025).

82. Sy, S. et al. Impacts of idealized land use and land management changes on weather extremes in West Africa. *Earth's Future* **13**(11), e2025EF006094. https://doi.org/10.1029/2025EF006094 (2025).

Acknowledgements
The West African Science Service Center on Climate Change and Adapted Land Use (WASCAL) program WACS-GRP under the auspices of the German Federal Ministry of Education and Research (BMBF) provided funding for this study. This work was part of the WASCAL CONCERT project (01LG2089A) and was provided with the necessary infrastructure to support both the field campaign and laboratory analysis at the KIT-Campus Alpin. Through the project '' Land Surface-Groundwater Interactions in West Africa: Impact of Land Use Changes on Groundwater Dynamics and land-atmosphere Exchange Processes, this study benefited from the support of the DAAD-Stiftung short-term research grant (57733724). We duly recognize the unwavering assistance offered by Kwesi D. Ochard from the WASCAL team in Bolgatanga (Ghana), and the Mole Park administration (Mr. Nichodemus L. Abatakanga) for the field campaign in the forest reserve. We appreciate the training and support offered by the Greenhouse Gas Determination in West Africa's Agricultural Landscapes (GreenGaDe) project through the Forestry Research Institute of Ghana (FORIG). The field campaign involved many individuals who could not be exhaustively listed.

Author contributions
F.E.O. and I.S. lead the field campaign with the support of R.S., F.N., S.G., M.A., A.F., P.D., E.Q., and L.H. The sample analysis at KIT laboratory was undertaken by A.S-S. with the support of R.K. and R.M. The funding was acquired by H.K., J.B., S.S., K.O., L.K.A., and C.F.O. The supervision was done by H.K., S.S., J.B., N.Y., Y.A-S., M.B. The manuscript's first draft was prepared by F.E.O. with the guidance of R.K. and S.S. The final version of the manuscript was revised by F.E.O., R.K., H.K., J.B., S.S., W.S., and I.S.

Declarations

Competing interests
The authors declare no competing interests.

Additional information
Supplementary Information The online version contains supplementary material available at https://doi.org/10.1038/s41598-026-36221-x.

Correspondence and requests for materials should be addressed to F.E.O. or H.K.

Reprints and permissions information is available at www.nature.com/reprints.

Publisher's note Springer Nature remains neutral with regard to jurisdictional claims in published maps and institutional affiliations.